THE UNIVERSITY OF CALGARY

Nonrelativistic and Scalar Relativistic Nuclear Spin-Spin Couplings in Density Functional Theory

By

Yang Khandogin

A THESIS SUBMITTED TO THE FACULTY OF GRADUATE STUDIES IN PARTIAL FULFILLMENT OF THE REQUIREMENTS FOR THE DEGREE OF MASTER OF SCIENCE

DEPARTMENT OF CHEMISTRY

CALGARY, ALBERTA

JULY, 1999

Abstract

Density functional theory based methodologies are applied to the study of nuclear spin-spin couplings. In the first part, an existing nonrelativistic implementation has been employed for the investigation of metal-ligand NMR coupling constants in a series of transition-metal systems. These include 3d-, 4d- and 5d-transition-metal carbonyl, oxo, fluoro, and phosphine complexes. By means of a molecular orbital-based analysis, insight into the origin of the Fermi-contact and paramagnetic spin-orbit coupling contribution has been gained. The experimental trends have also been rationalized in terms of simple criteria that can help to qualitatively predict the magnitude of the coupling constants. In the second part, two approximate frozen-core relativistic correction schemes have been developed and evaluated on one-bond couplings to heavy main-group and transition-metal atoms. The second correction scheme, which only accounts for the relativistic contraction of s orbitals at the heavy metal nucleus, can satisfactorily recover the relativistic increase on the metal-ligand coupling constants for both main-group and transition-metal systems. The connection between the *trans* influence and coupling constants has been found to be mainly of electronic nature and can be rationalized using a perturbation theory-based molecular orbital approach.

Table of Contents

Acknowledgements

I wish to take this opportunity to thank my supervisor, Professor Tom Ziegler, for introducing me to the fascinating and fruitful field of applied quantum chemistry. I am also thankful for his guidance and advice.

I would like to thank Professors Arvi Rauk, Hans Laue, and Deborah Hearn, from whose wonderful lectures I have benefited a lot. I also wish to thank Professors Brian Keay and Tris Chivers for their support and advice.

I have enjoyed the period working in the Z-team. I wish to thank Drs. Serge Patchkovskii, Steve Wolff, Georg Schreckenbach, Cory Pye, Artur Michalak, Rochus Schmid, and Professor Tom Gilbert for valuable discussions and sharing their experience with me. I want to include special thanks to my office mate Dr. Cory Pye for making the limited space pleasant and enjoying the same heavy music with me. I also want to add my sincere thanks to Dr. Liqun Deng for his encouragement and support. I would like to extend my thanks to all other members in the group.

I am also indebted to all my friends, Sandi, Ramon, Bodo, Jingbo, and Silja, for their friendship, support, and especially the memorable time we spent together.

This work would be impossible without the endless love, support and inspiration from my wonderful partner and husband Igor. In this category, I would also like to thank my mom and dad for their love and support.

FOR MY FAMILY

List of Tables

List of Figures

List of Abbreviations

ADF	Amsterdam Density Functional
AE	All electron
AO	Atomic orbital
Ax	Axial
Dar	Darwin
DFT	Density functional theory
DSO	Diamagnetic spin-orbit
Eq.	equation
eq	equatorial
ESR	Electron magnetic resonance
Exp.	Experiment
FC	Fermi-contact
FRC	Frozen core
GGA	Generalized gradient approximation
HF	Hartree-Fock
I/O	Input/output
KS	Kohn-Sham
LDA	Local density approximation
MCSCF	Multi-configurational self consistent
MO	Molecular orbital
MV	Mass-velocity
NMR	Nuclear magnetic resonance
NR	nonrelativistic
occ	occupied
PSO	Paramagnetic spin-orbit
QR	Quasi-relativistic
Ref.	Reference
RPA	Random-phase approximation

SD	Spin-dipolar
SI	*Le Système International*
SO	Spin-orbit
SR	Scalar relativistic
SRI	Scalar relativistic correction scheme I
SRII	Scalar relativistic correction scheme II
vir	virtual
XC	Exchange-correlation
ZORA	Zeorth order regular approximation

Die wissenschaftliche Begriffsbildung und Methode unterscheidet sich von der des Alltags lediglich durch größere Schärfe der Begriffe und Schlüsse, durch sorgfältigere und systematischere Auswahl des Erfahrungsmaterials sowie durch Sparsamkeit im logischen Sinne.

Albert Einstein: Aus meiner späten Jahren

Chapter 1
Introduction

1.1 Motivation and Objectives

Over the last two decades, *Density Functional Theory* (DFT) has established itself as a powerful and flexible tool in investigations of a wide range of chemical and physical phenomena. Traditionally, it has been applied to calculations of molecular structure, bonding energies and reaction pathways. Yet, the potential of this promising electron structure theory has not been fully explored. New application fields such as second-order magnetic properties (for example, NMR shifts[1] and coupling parameters[2] have recently emerged. NMR spectroscopy is among the most important tools in the contemporary chemist's kit. Because of the extraordinary sensitivity of the shift and coupling parameters to small chemical changes, a first-principles quantum mechanical study is often desirable for their prediction and interpretations.

The goal of this work is to develop and apply DFT based techniques to the study of NMR spin-spin coupling constants. Presented here is a thesis consisting of two major parts. In the first part, an existing DFT based nonrelativistic nuclear coupling implementation is applied to NMR coupling constants in a variety of 3d-, 4d- and 5d-transition-metal systems. The purpose of this part of the study is to validate the current nonrelativistic methodologies and to rationalize the experimental observations. The latter is made possible by the molecular orbital-based analysis of the principal contributions. The second part of the thesis deals with two approximate frozen-core scalar relativistic correction schemes. These relativistic corrections are evaluated on one-bond spin-spin coupling constants involving heavy main-group and transition-metal elements. The intention of this part of the work is to develop some simple schemes to account for the major relativistic effects on the spin-spin coupling, and to apply them to the systems of our major interest: heavy transition-metal complexes. From the point of view of a theoretical chemist, the ultimate goal of the thesis is to contribute to the understanding of

the electron-coupled nuclear spin-spin coupling phenomenon and the manifestation of electronic effects of relativity in this property. For a practical chemist, the presented work is aimed at providing some rationales on theoretical footings that can help in understanding the structure-coupling relation and possibly make predictions.

1.2 Kohn-Sham Density Functional Theory

Density functional theory (DFT)[3] is based on the theorem of Hohenberg and Kohn, which states that the ground state energy of an electronic system is uniquely determined by the electron density:

$$E \equiv E[\rho(\vec{r})]. \tag{1.1}$$

The electron density represents the number of electrons per unit volume and is uniquely defined by the wavefunction:

$$\rho(\vec{r}_1) = N\int\cdots\int|\Psi(\vec{x}_1,\vec{x}_2,\ldots\vec{x}_N)|^2 ds_1 d\vec{x}_2\cdots d\vec{x}_N. \tag{1.2}$$

Electron density can be put in the place of wavefunction as a basic variable in describing the electron structure. Further, DFT by Hohenberg and Kohn expresses the total electronic energy as:

$$E[\rho] = T_0[\rho] - \sum_{A=1}^{Nuc}\int d\vec{r}_1 \frac{Z_A}{|\vec{r}_1-\vec{R}|}\rho(\vec{r}_1) + \frac{1}{2}\int d\vec{r}_1 d\vec{r}_2 \frac{\rho(\vec{r}_1)\rho(\vec{r}_2)}{|\vec{r}_1-\vec{r}_2|} + E_{XC}[\rho(\vec{r}_1)]. \tag{1.3}$$

Here, the first term is the kinetic energy of the non-interacting electrons with the same density as the interacting system, the second term represents the nuclear-electron attraction, the third term is the classical electron-electron Coulomb repulsion, and the last term represents the exchange-correlation (XC) energy functional, whose exact form remains unknown and only approximations are available.

Based on the Variational principle, the optimal density that minimizes the total energy can be found by solving a set of Kohn-Sham (KS) equations:

$$\hat{h}[\rho]\psi_i = \varepsilon_i\psi_i. \tag{1.4}$$

The electron density is then given in terms of the eigenfunctions, referred to as KS molecular orbitals, as:

$$\rho(\vec{r}_1) = \sum_{i=1}^{occ} \psi_i(\vec{r}_1)\psi_i^*(\vec{r}_1). \tag{1.5}$$

The KS operator $\hat{h}[\rho]$ is given by:

$$h[\rho(\vec{r}_1)] = \frac{\nabla^2}{2} + \sum_{A=1}^{N_{nuc}} \frac{Z_A}{|\vec{r}_1 - \vec{R}_A|} + \int d\vec{r}_2 \frac{\rho(\vec{r}_2)}{|\vec{r}_1 - \vec{r}_2|} + V_{XC}[\rho(\vec{r}_1)], \tag{1.6}$$

where the first term represents the kinetic energy operator, the second term represents the nuclear potential, the third term represents the Coulomb potential, and last term is the exchange correlation potential obtained as the functional derivative of the XC energy $E_{xc}[\rho]$:

$$V_{XC}[\rho] = \frac{\delta E_{XC}[\rho]}{\delta \rho}. \tag{1.7}$$

Because of its lower computational demands and yet sufficient accuracy, Kohn-Sham DFT has become a method of choice over the traditional highly correlated *ab initio* theory in studying medium to large-sized chemical systems. The Amsterdam density functional package (ADF)[4,5] is a DFT code developed in both the Vrije Universitet Amsterdam and the University of Calgary. It makes extensive use of Slater-type basis functions and the recently developed advanced numerical techniques. ADF has proven to be one of the most successful DFT tools in serving the needs of computational chemistry both in academia and in industry.

1.3 Double Perturbation Theory and Second-Order Properties

Often encountered in chemistry are effects arising from two simultaneous perturbations to the total electronic energy. The associated second-order properties can be viewed theoretically as the second-order derivative of energy with respect to two (external or internal) parameters:

$$P = \left.\frac{\partial^2 E}{\partial \lambda_1 \lambda_2}\right|_{\lambda_1=\lambda_2=0}. \tag{1.8}$$

Examples of chemically relevant second-order properties are: NMR chemical shifts and ESR g-tensors (λ_1=external magnetic field, λ_2=nuclear or electronic spin magnetic

moment); NMR nuclear-nuclear couplings and ESR hyperfine couplings (λ_1=nuclear spin magnetic moment, λ_2=nuclear or electronic spin magnetic moment); harmonic force constants (λ_1, λ_2=nuclear displacements); electric polarizability (λ_1, λ_2=external electric field); and diamagnetism (λ_1, λ_2=external magnetic field).

On the basis of Hellmann-Feynman theorem, the double perturbation theory is developed to deal with these properties quantum mechanically. Thus, a second-order property P can be written as:

$$P = \frac{\partial^2}{\partial\lambda_1\partial\lambda_2}\langle\Psi|H|\Psi\rangle = \frac{\partial}{\partial\lambda_1}\left\langle\Psi\left|\frac{\partial H}{\partial\lambda_2}\right|\Psi\right\rangle$$
$$= \left\langle\frac{\partial}{\partial\lambda_1}\Psi\left|\frac{\partial H}{\partial\lambda_2}\right|\Psi^0\right\rangle + \left\langle\Psi^0\left|\frac{\partial H}{\partial\lambda_2}\right|\frac{\partial}{\partial\lambda_1}\Psi\right\rangle + \left\langle\Psi^0\left|\frac{\partial^2 H}{\partial\lambda_1\partial\lambda_2}\right|\Psi^0\right\rangle \qquad (1.9)$$

Here in the first step, use is made of Hellmann-Feynman theorem (see Discussions in ref 3). Eq. (1.9) shows that in order to calculate a second-order property, one has to calculate the first-order change in the wavefunction due to one perturbation. This can be obtained via analytical approaches such as the coupled perturbed Hartree-Fock and the uncoupled perturbed Kohn-Sham method or via a finite perturbation approach. The details of the uncoupled perturbed Kohn-Sham method as well as the finite perturbation approach are given in Chapter 2.

1.4 The NMR Spin-Spin Coupling Code

The nonrelativistic NMR spin-spin coupling code was developed and implemented by Ross Dickson within the ADF package version 1.1.[2] This program has been modified and ported to the more recent release of ADF: ADF 2.3.3. While the key functionality is maintained, alterations have been introduced partly to fix known bugs but more importantly to perform efficient I/O and memory handling as well as to adapt to the new features of the standard ADF package. Below is the outline of the spin-spin coupling code within ADF. As shown, the three contributions to the total spin-spin coupling tensor are computed separately. A detailed technical description can be found elsewhere.[6]

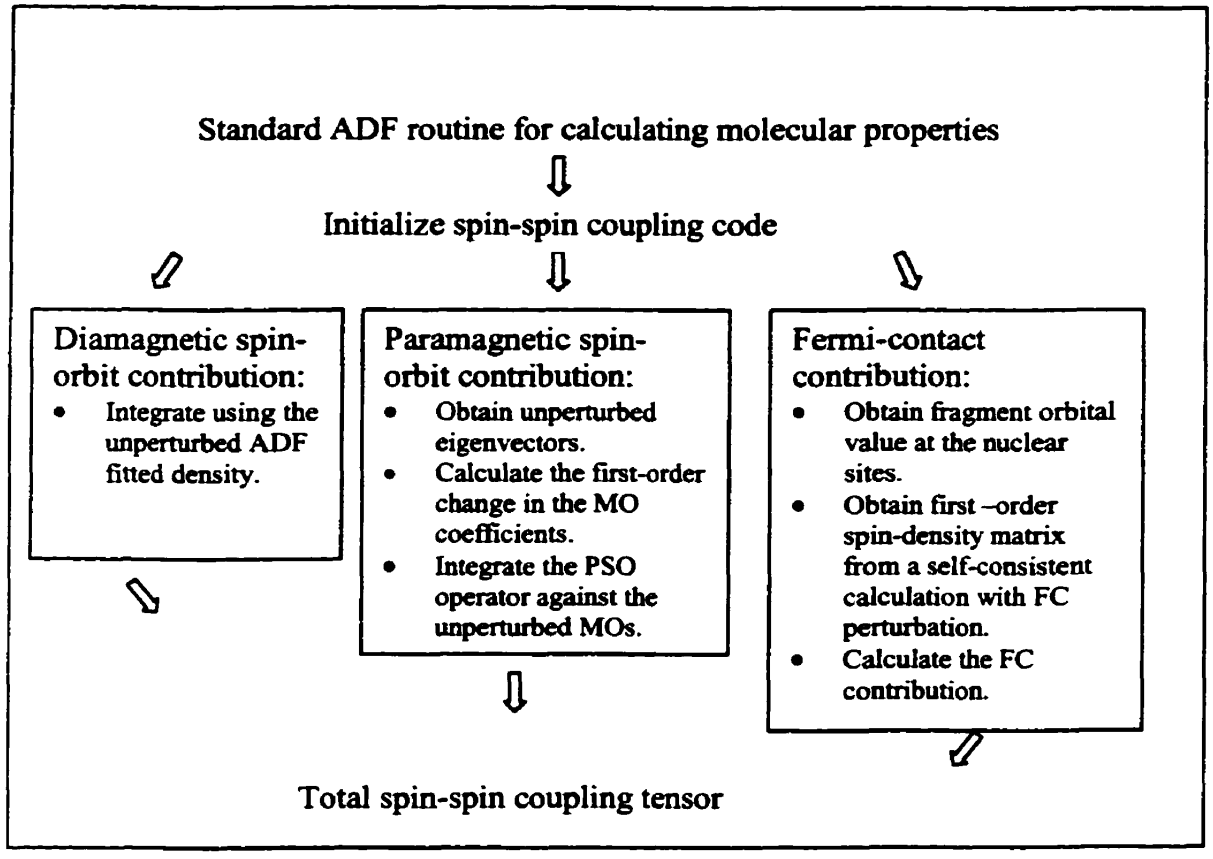
Standard ADF routine for calculating molecular properties
Initialize spin-spin coupling code
Diamagnetic spin-orbit contribution:
• Integrate using the unperturbed ADF fitted density.
Paramagnetic spin-orbit contribution:
• Obtain unperturbed eigenvectors.
• Calculate the first-order change in the MO coefficients.
• Integrate the PSO operator against the unperturbed MOs.
Fermi-contact contribution:
• Obtain fragment orbital value at the nuclear sites.
• Obtain first –order spin-density matrix from a self-consistent calculation with FC perturbation.
• Calculate the FC contribution.
Total spin-spin coupling tensor

Chapter 2

Nonrelativistic Nuclear Spin-spin Couplings: A DFT study of NMR Coupling Constants in Transition-Metal Systems

2.1 Introduction

The observation of couplings between nuclear spins on different nuclei as recorded in nuclear magnetic resonance experiments is used extensively to deduce molecular structures and other properties of chemical interest. The full quantum mechanical treatment of nuclear spin-spin coupling was first formulated by Ramsey[7] based on perturbation theory. In this nonrelativistic formulation the coupling has four contributions from respectively: (1) Fermi-contact (FC), (2) paramagnetic spin-orbit coupling (PSO), (3) diamagnetic spin-orbit coupling (DSO) and (4) spin-dipolar (SD) interactions. The theory has later been refined by others[8] and modified to include relativistic effects[9].

Earlier semi-empirical studies[10-13] were able to differentiate the magnitude of the four contributions and give semi-quantitative results for couplings between the light nuclei in some organic and inorganic systems. More recently use has been made of *ab initio* methods[8,14-16] in studies of spin-spin coupling and quantitative results have been obtained in cases where most of electron correlation has been taken into account.

Density functional theory has emerged as a tangible alternative to traditional *ab initio* methods since it is able to include electron correlation in a computationally efficient way that makes it possible to treat even large size molecules quantitatively. The use of DFT in spin-spin coupling calculations was pioneered by Malkin et al.[17,18] in an implementation based on Gaussian orbitals within the deMon program system. Subsequently, Dickson and Ziegler[2] presented an implementation into the Amsterdam density functional package (ADF) based on Slater type orbitals.

Malkin et al.[17,18] have examined the performance of their methodology on some organic and main group inorganic molecules. Their conclusion is that the current method

based on DFT yields very reliable results for lighter main group elements. The same conclusion was reached by Dickson and Ziegler[2]. The latter authors were further able to present promising results for couplings between carbon and some 3d-transition-metal nuclei.

The objective of the present study has been to extend the work by Dickson and Ziegler[2] on metal-ligand spin-spin coupling. For this purpose, we choose to calculate a large number of experimentally known one-bond reduced coupling constants ^1K(M-X) in small to medium sized carbonyl, oxo, fluoro and phosphine complexes of 3d-, 4d-, and 5d-metals. In particular, we shall analyze the Fermi-contact and paramagnetic spin-orbit coupling contributions in terms of the molecular orbitals and provide a theoretical rationalization for the observed periodic trends in the reduced coupling constants. We shall further analyze the core and valence orbital contributions to the Fermi-contact term and discuss the applicability of neglecting core polarization by using core orbitals from atomic calculations. Finally, we will demonstrate the significant improvement of the calculated coupling constants in 4d- and especially 5d-transition-metal systems by adopting a quasi-relativistic treatment[19-22] and conclude with the need for more elaborate relativistic models.

2.2 Computational Method and Details

The way in which spin-spin couplings are calculated in the ADF program has already been sketched in the original work by Dickson and Ziegler.[2] We shall in the following provide a more comprehensive account of the approximations involved as well as a detailed discussion of the special assumptions that are unique to DFT.

2.2.1 General Formulation

A nucleus G with the intrinsic angular momentum $\vec{I}_G$ has an associated magnetic dipole $\vec{\mu}_G$ given by

$$\vec{\mu}_G = \frac{\hbar}{2\pi}\vec{I}_G\gamma_G, \tag{2.1}$$

where • is Planck's constant divided by 2π and γ_G is the experimentally obtained magnetogyric ratio between $\vec{I}_G$ and $\vec{\mu}_G$. The dependence of the total electronic energy on the nuclear magnetic moments can be expressed as[7,8] a simple Taylor expansion

$$E = E^0 + \sum_A \sum_{i=1}^{3} \left.\frac{dE}{d\mu_A^i}\right|_{(\mu_A=0)} \mu_A^i + \frac{1}{2}\sum_A \sum_B \sum_{i=1}^{3}\sum_{j=1}^{3} \left.\frac{d^2E}{d\mu_A^i d\mu_B^j}\right|_{(\mu_A^i=\mu_B^j=0)} \mu_A^i \mu_B^j + O(3), \tag{2.2}$$

where i and j runs over the cartesian components and E^o is the electronic energy in absence of the magnetic interaction from the nuclear magnetic moments. The second derivative for $A \neq B$ is often referred to as the reduced coupling constant[7,8]

$$K(A,B)_{ij} = \left.\frac{d^2E}{d\mu_A^i d\mu_B^j}\right|_{(\mu_A^i=\mu_B^j=0)}, \tag{2.3}$$

for which the trace

$$K = \frac{1}{3}\left(K_{xx} + K_{yy} + K_{zz}\right) \tag{2.4}$$

is the reduced spin-spin coupling constant of NMR spectroscopy.

The electronic energy in DFT[23,24,3,25] can, in the absence of magnetic interactions, be written as

$$\begin{aligned} E^o[\Phi_i^o] = \sum_i^{occ} \int d\vec{r}_1 (\Phi_i^o)^* \frac{p^2}{2}\Phi_i^o + \int d\vec{r}_1 V(\vec{r}_1)\rho^o(\vec{r}_1) \\ + \frac{1}{2}\int d\vec{r}_1 d\vec{r}_2 \frac{\rho^o(\vec{r}_1)\rho^o(\vec{r}_2)}{|\vec{r}_1 - \vec{r}_2|} + E_{XC}^o[\rho^o] \end{aligned}, \tag{2.5}$$

where

$$\rho^o = \sum_i^{occ} \Phi_i^o (\Phi_i^o)^* \tag{2.6}$$

represents the electron density of the n-electron system and $\{\Phi_i^0\}$ is a set of n orthonormal and occupied (occ) one-electron functions.

The first term in Eq. (2.5) represents the kinetic energy of a model system with the same density, but without electron-electron interactions. The second term describes the interaction of the electrons with the external (nuclear) potential $V(\vec{r}_1)$. The third term is the so-called Hartree term. It describes the interaction of the electron density with itself. The exchange-correlation (XC) energy E_{XC}^0 is a functional of the electron density. E_{XC}^0 contains the difficulties of the many-electron problem, and some approximation has to be used, as will be specified in the section on computational details.

It is now possible to derive one-electron equations, the so-called Kohn-Sham (KS) equations[24], from the energy expression Eq. (2.5)

$$\hat{h}^o[\rho^o]\Psi_i^o = \varepsilon_i^o\Psi_i^o \tag{2.7}$$

where

$$\hat{h}[\rho^0(\vec{r}_1)] = \frac{p^2}{2} + V(\vec{r}_1) + \int d\vec{r}_2 \frac{\rho^0(\vec{r}_2)}{|\vec{r}_1 - \vec{r}_2|} + V_{XC}^0[\rho^0(\vec{r}_1)]. \tag{2.8}$$

Furthermore, the XC potential V_{XC}^o is the functional derivative[24] of the XC energy E_{XC}^o:

$$V_{XC}^o(\vec{r}_1) \equiv \frac{\delta E_{XC}^o[\rho]}{\delta\rho}. \tag{2.9}$$

The KS equations are derived under the condition that the n occupied solutions $\{\Phi_i^0\}$ with the lowest eigenvalues $\{\varepsilon_i^0\}$ minimize the energy expression of Eq. (2.5). The solutions to Eq. (2.7) with eigenvalues $\{\varepsilon_i^0\}$ of higher energy are referred to as virtual orbitals (vir). In order to evaluate the energy derivatives of Eq. (2.2), magnetic terms must be introduced into the many-electron Hamiltonian that couple the nuclear magnetic moments to the electronic degrees of freedom[26-28]. These terms must further be linear in one of the magnetic moments corresponding to nuclei A and B, $\hat{h}^{\vec{\mu}_A}$, $\hat{h}^{\vec{\mu}_B}$ or bilinear in both, $\hat{h}^{\vec{\mu}_A\cdot\vec{\mu}_B}$. After the introduction of the magnetic terms the total energy reads

$$E = E^o[\Phi_i] + \sum_i^{occ} \int d\vec{r}_1 \Phi_i^*[\hat{h}^{(\vec{\mu}_A)} + \hat{h}^{(\vec{\mu}_B)} + \hat{h}^{(\vec{\mu}_A \cdot \vec{\mu}_B)}]\Phi_i \tag{2.10}$$

where $\{\Phi_i\}$ is obtained from the new set of KS equations

$$\hat{h}\Psi_i = \{\hat{h}^o[\rho] + \hat{h}^{(\vec{\mu}_A)} + \hat{h}^{(\vec{\mu}_B)} + \hat{h}^{(\vec{\mu}_A \vec{\mu}_B)}\}\Psi_i = \varepsilon_i \Psi_i. \tag{2.11}$$

We note that E^0 in Eq. (2.10) and $\hat{h}^0$ in Eq. (2.11) can now be expressed in terms of the occupied solutions $\{\Phi_i\}$ to Eq. (2.10), and the associated density

$$\rho = \sum_i^{occ} \Psi_i \Psi_i^*. \tag{2.12}$$

Also, we assume that the functional dependence of E_{xc} on the density is unchanged by the introduction of magnetic terms and that E_{xc} has no current density dependence:

$$E_{xc}[\rho, \vec{J}] \cong E_{XC}^o[\rho] \tag{2.13}$$

By substituting E of Eq. (2.10) into Eq. (2.3) we obtain the following expression for the reduced coupling tensor

$$\begin{aligned} K(A,B)_{ij} = & \sum_k^{occ} \int \left(\Phi_k^{(\mu_A^i)}(\vec{r})\right)^* [d\hat{h}^{\vec{\mu}_B} / d\mu_B^j] \Phi_k^0(\vec{r}) d\vec{r} \\ & + \sum_k^{occ} \int \left(\Phi_k^0(\vec{r})\right)^* [d\hat{h}^{(\vec{\mu}_B)} / d\mu_B^j] \Phi_k^{(\mu_A^i)}(\vec{r}) d\vec{r} \\ & + \sum_k^{occ} \int \left(\Phi_k^0(\vec{r})\right)^* [d^2(\hat{h}^{(\vec{\mu}_A \cdot \vec{\mu}_B)}) / d\mu_A^i d\mu_B^j] \Phi_k^0(\vec{r}) d\vec{r} \end{aligned} , \tag{2.14}$$

where we have used that

$$\left.\frac{dE^o[\Phi]}{d\mu_G^l}\right|_{(\mu_{G=0}^l)} = 0 \quad \{G = A, B; l = x, y, z\}, \tag{2.15a}$$

since $E^0[\Phi^0]$ of Eq. (2.5) is determined variationally. Further, we have introduced the notation

$$\Phi^{(\mu_G^k)} = \left(d\Phi / d\mu_G^k\right)_{(\mu_G^k=0)} (G = A, B; k = x, y, z). \tag{2.15b}$$

There are four terms[26-28] that contribute to the magnetic terms in Eq. (2.11). Three are linear in the magnetic moment

$$\hat{h}^{FC} = \frac{4\mu_0\beta}{3}\delta(r_A = 0)\cdot\vec{S}\cdot\vec{\mu}_A \tag{2.16a}$$

$$\hat{h}^{PSO} = \frac{\mu_0\beta}{2\pi i}\frac{1}{r_A^{\,3}}\vec{\mu}_A\cdot(\vec{r}_A\times\vec{\nabla}) \tag{2.16b}$$

$$\hat{h}^{SD} = \frac{\mu_0\beta}{2\pi}\left(\frac{3(\vec{S}\cdot\vec{r}_A)(\vec{\mu}_A\cdot\vec{r}_A)}{r_A^{\,5}} - \frac{\vec{S}\cdot\vec{\mu}_A}{r_A^{\,3}}\right) \tag{2.16c}$$

and one is bilinear

$$\hat{h}^{DSO} = \frac{\mu_0^{\,2}e\beta}{(4\pi)^2}\cdot\frac{(\vec{\mu}_A\cdot\vec{\mu}_B)(\vec{r}_A\cdot\vec{r}_B) - (\vec{\mu}_A\cdot\vec{r}_B)(\vec{\mu}_B\cdot\vec{r}_A)}{r_A^{\,3}r_B^{\,3}}. \tag{2.16d}$$

In the equations above, μ_0 is the permeability of the vacuum, β is the Bohr magneton, and $\vec{r}_G$ is the position vector of the electron with respect to nucleus G. Each of the four terms will contribute to the reduced coupling constant tensor

$$K(A,B)_{ij} = K(A,B)_{ij}^{FC} + K(A,B)_{ij}^{PSO} + K(A,B)_{ij}^{DSO} + K(A,B)_{ij}^{SD}. \tag{2.17}$$

Since the spin-dipolar contribution $K(A,B)_{ij}^{SD}$ is usually very small[13], it will not be considered further in the present work. However, we shall now in turn discuss the evaluation of the remaining three terms in Eq. (2.17). The discussion will be restricted to the diagonal terms $K(A,B)_{ii}$ for which experimental data are available primarily in terms of the reduced coupling constant of Eq. (2.4).

2.2.2 Diamagnetic spin-orbit term

The diamagnetic spin-orbit coupling Hamiltonian $\hat{h}^{DSO}$ of Eq. (2.16d) is bilinear in the magnetic moments on A and B. We can, as a consequence of Eq. (2.14), write its contribution $K(A,B)_{ii}^{DSO}$ to the coupling constant of Eq. (2.4) directly in terms of the unperturbed KS orbitals of Eq. (2.7) as

$$K(A,B)_{ii}^{DSO} = \frac{\mu_0{}^2 e^2}{16\pi^2 m_e} \sum_k^{occ} \int \left(\Phi_k^o(\vec{r}_1)\right)^* \left[\frac{(\vec{r}_A \cdot \vec{r}_B) - r_A^i r_B^i}{r_A{}^3 r_B{}^3}\right] \Phi_k^o(\vec{r}_1) d\vec{r}_1 \quad \text{with i} \in \{x,y,z\} \tag{2.18}$$

The component $K(A,B)_{ii}^{DSO}$ is related to the interaction energy between the diamagnetic orbital current density induced by the first nucleus and the magnetic nuclear dipole of the second nucleus.

2.2.3 Paramagnetic spin-orbit term

The operator $\hat{h}^{PSO}$ from the paramagnetic spin-orbit coupling term is linear in the nuclear magnetic moment. Thus, according to Eq. (2.14) the evaluation of $K(A,B)_{ii}^{PSO}$ requires the specification of the first-order change to the KS orbitals, $\Phi_k^{(\mu_{A,PSO}^i)}$, induced by $\hat{h}^{PSO}$.

We can obtain $\Phi_k^{(\mu_{A,PSO}^i)}$ from Eq. (2.11) by collecting all terms that are first order in the perturbation $\hat{h}^{PSO}$ and solve for $\Phi_k^{(\mu_{A,PSO}^i)}$ as a linear combination of the unperturbed KS orbitals Φ_k^0. We obtain in this way by standard technique[28]

$$\Phi_k^{(\mu_{A,PSO}^i)} = \sum_{l \neq k}^{occ+vir} \frac{\int \left(\Phi_k^0(\vec{r})\right)^* \hat{h}^{(\mu_{A,PSO}^i)} \Phi_l^0(\vec{r}) d\vec{r}}{\varepsilon_k^o - \varepsilon_l^o} \Phi_l^0(\vec{r}). \tag{2.19}$$

In Eq. (2.19) the summation over *l* includes both occupied and virtual zeroth-order KS orbitals. We note that c is purely imaginary, since $\hat{h}^{PSO}$ is purely imaginary and all zeroth-order KS orbitals are real. Purely imaginary first order changes in the orbitals do not change the total electron density to first order. There is as a consequence no first-order contribution from $\hat{h}^0[\rho]$ of Eq. (2.8). Such a first-order contribution would have

been possible if we had avoided the approximation to E_{xc} in Eq. (2.13) and allowed for a specific current density dependence[29,30].

Finally a substitution of $\Phi_k^{(\mu_A^i,PSO)}$ from Eq. (2.19) into Eq. (2.14) allows us to write

$$K(A,B)_{ii}^{PSO} = 2\sum_{k}^{occ}\sum_{l}^{vir}\frac{\left(\int\left(\Phi_k^o(\vec{r})\right)^* \hat{h}^{(\mu_A^i,PSO)}\Phi_l^o(\vec{r})d\vec{r}\int\left(\Phi_l^o(\vec{r})\right)^* \hat{h}^{(\mu_B^i,PSO)}\Phi_k^o(\vec{r})d\vec{r}\right.}{\varepsilon_k^o-\varepsilon_l^o}. \qquad (2.20)$$

Here $K(A,B)_{ii}^{PSO}$ is related to the interaction energy between the paramagnetic current density induced by one nuclear magnetic dipole with another magnetic nuclear dipole. Note that we have omitted the occupied orbitals in the summation over l since this summation has zero contribution to the coupling.

2.2.4 Fermi-contact term

Evaluation of $K(A,B)_{ii}^{FC}$ from the Fermi-contact operator $\hat{h}^{FC}$ requires again a specification of the first order change in the KS orbitals, $\Phi_k^{(\mu_A^i,FC)}$, since $\hat{h}^{FC}$ is linear in the nuclear magnetic moment. We can find $\Phi_k^{(\mu_A^i,FC)}$ from

$$\left\{\hat{h}^0[\rho]+\frac{4\mu_0\beta}{3}\hat{S}_i\cdot\mu_A^i\delta(r_A=0)\right\}\Phi_k=\varepsilon_k\Phi_k \qquad (2.21)$$

by collecting terms to first order in μ_A^i. The operator $\hat{h}^{FC}$ is real and will as a consequence induce a real first-order change in the density as well as in $\hat{h}^0[\rho]$. Thus, finding $\Phi_k^{(\mu_A^i,FC)}$ from Eq. (2.21) by collecting first-order terms will lead to a set of coupled perturbed equations, which will require a special programming effort[29,30,14-16] to solve.

Alternatively, we might make use of finite perturbation theory and solve Eq. (2.21) self-consistently by adding $\hat{h}^{FC}$ to $\hat{h}^0[\rho]$ in our standard ADF program with a minimum of effort. The execution of two separate SCF calculations with Φ_k^0 as the basis and μ_A^i in $\hat{h}^{FC}$ represented by respectively λ and $-\lambda$ affords the solutions $\Phi_k(\lambda)$ and

$\Phi_k(-\lambda)$ respectively, where λ is a perturbation parameter. The two solutions allow us to obtain $\Phi_k^{(\mu^i_{A,FC})}$ as

$$\Phi_k^{(\mu^i_{A,FC})} \equiv \left(d\Phi_k / d\mu^i_A\right)_{(\mu^i_{A=0})} = \left(d\Phi_k(\lambda)/d\lambda\right)_{(\lambda=o)} \equiv \frac{\Phi_k(\lambda)-\Phi_k(-\lambda)}{2\lambda} = \sum_l^{occ+vir} U_{kl}^{(\mu^i_{A,FC})}\Phi_l^o. \tag{2.22}$$

The original zeroth order basis Φ_k^0 is normally expressed in terms of a product of spin and space functions $\Phi_k^0 = \phi_k^0\gamma_z$, where γ_z is an eigenfunction to the z-component $\hat{S}_z$ of the spin operator $\hat{\vec{S}}$. By a unitary transformation of $\Phi_k^0 = \Phi_{k,z}^0 = \phi_k^0\gamma_z$, we can generate an equivalent zeroth-order basis, $\Phi_{k,i}^0 = \phi_k^0\gamma_i$, where $\Phi_{k,z}^0$ and $\Phi_{k,i}^0$ have the same spatial parts, ϕ_k^0, whereas their spin parts, γ_z and γ_i, are eigenfunctions to respectively $\hat{S}_z$ and $\hat{S}_i$ with the same eigenvalues. It is thus clear that solving Eq. (2.20) for the three different components i=x,y,z with the corresponding basis $\Phi_k^0 = \phi_k^0\gamma_z$ (i=x,y,z) will afford the same expansion coefficients $U_{kl}^{(\mu^i_{A,FC})}$ and spatial orbital parts for $\Phi_k^{(\mu^i_{A,FC})}$ with i=x,y,z. This is a simple consequence of the fact that the spatial part of Eq. (2.20) will be the same for i=x,y,z. Thus,

$$\Phi_k^{(\mu^i_{A,FC})} = \sum_l^{occ+vir} U_{kl}^{(\lambda)}\phi_i^o\gamma_i \quad (i = x, y, z). \tag{2.23}$$

As a consequence of Eq. (2.23) only two SCF calculations are required to determine all three components of $\Phi_k^{(\mu^i_{A,FC})}$ with i=x,y,z. A substitution of $\Phi_k^{(\mu^i_{A,FC})}$ from Eq. (2.23) into Eq. (2.14) finally allows us to write

$$K(A,B)_{ii}^{FC} = 2\sum_k^{occ}\sum_l^{vir} U_{kl}^{(\mu^i_{A,FC})}\int\Phi_l^o(\vec{r}_B)[\frac{4\mu_o\beta}{3}\hat{S}_i\cdot\mu_B^i\hat{\delta}(r_B=o)]\Phi_k^o(\vec{r}_B)d\vec{r}_B. \tag{2.24}$$

The accuracy by which $\Phi_k^{(\mu^i_{A,FC})}$ is determined from the finite perturbation expression in Eq. (2.22) depends on an appropriate choice of the parameter λ. Too large a value of λ introduces higher order terms into the difference of Eq. (2.22). On the other hand, numerical errors in the determination of $\Phi_k(\lambda)$ and $\Phi_k(-\lambda)$ from the numerical

integration used in ADF as well as the SCF convergence will be amplified in the calculation of $\Phi_k^{(\mu^1_{A,FC})}$ if λ is too small. We found $\lambda = 10^{-3}$ to be an optimal value in connection with a SCF convergence threshold of 10^{-4} for the density matrix and an integration accuracy of 10^{-5} for the KS matrix elements.

In Eqs. (2.22) and (2.23), nucleus A is the perturbing center whereas B is the responding nucleus. We can in principle choose either the metal or the ligand center as the perturbing atom. In practice the calculated value for $K(A,B)_{ii}^{FC}$ will depend somewhat on the choice of the perturbing atom due to numerical inaccuracies. We find the choice of the perturbing atom to have a small effect (less than 3%) for complexes of 3d and 4d elements whereas the difference is much larger for 5d elements. We have in the following chosen the ligand center as the perturbing atom since it gives rise to results that are numerically stable with respect to reasonable variations in λ as well as the parameters for the numerical accuracy and the SCF convergence threshold.

2.2.5 Computational Details

We performed all calculations using the nuclear spin-spin coupling code[2] incorporated into the ADF[31-34]. The self-consistent DFT calculations were carried out based on the local exchange-correlation potential due to Vosko, Wilk and Nusair[35] augmented with Becke's nonlocal exchange correction[122] and Perdew's nonlocal correlation correction[123]. Unless otherwise specified, we used uncontracted double-ζ core and triple-ζ valence basis[36] for all atoms in the all-electron calculations and a triple-ζ valence basis in the frozen-core calculations. The metal center valence space included *n*s, np, *n*d, and (*n*+1)s shells. The integration and SCF convergence parameters were set to 10^{-5} and 10^{-4}, respectively. Structures used were taken from experimental results if available. In the finite difference calculations of the FC term, we chose the lighter atom as the perturbing center and used 10^{-3} for the perturbation parameter. Since the sign of coupling constants are not always experimentally available, we only compare the absolute value of calculated and measured coupling constants.

2.3 Results and Discussion

2.3.1 Transition-metal carbonyls

Table 2.1 compares our calculated metal-carbon nuclear coupling constants for 3d-, 4d- and 5d-transition metal carbonyls to experimental values[37,38]. For the 3d-complexes we contrast the results from all-electron (AE) and frozen-core (FRC) calculations. For the 4d- and 5d- complexes the comparison is between results from nonrelativistic and quasirelativistic (QR) calculations. The calculated coupling constants for the 3d-complexes are in good agreement with experiment whereas the theoretical estimates for the 4d- and 5d- complexes are consistently smaller than the experimental values, especially without the inclusion of relativistic effects.

An analysis of the calculated coupling constants for the transition metal carbonyl systems reveals that the Fermi-contact coupling term dominates whereas contributions from the spin-orbit coupling terms amount to less than a few percent. Thus, our analysis of the calculated coupling constants for the carbonyls will be restricted to the Fermi-contact term.

The major part of $K(A,B)_{ii}^{FC}$, Eq. (2.24), can be written directly in the uncoupled form by neglecting any contribution from first order changes to $\hat{h}^0$, Eq. (2.8), induced by $\hat{h}^{FC}$ as

$$K(A,B)_{ii}^{FC} \cong 2\left(\frac{2\mu_o\beta}{3}\right)^2 \sum_{k}^{occ}\sum_{l}^{vir} \frac{\int \Phi_l^o \delta(r_A = o)\Phi_k^o d\bar{r}_A \int \Phi_l^o \delta(r_B = o)\Phi_k^o d\bar{r}_B}{\varepsilon_k^o - \varepsilon_l^o}. \quad (2.25)$$

Table 2.1 Reduced coupling constants[h] K(M-C) in some 3d-, 4d- and 5d-transition-metal carbonyls.

molecule	FRC	AE	$r_{M\text{-}C}$ (Å)	$K^{Exp.}$
$V(CO)_6^-$	158	129	1.968[a]	146[f]
$Fe(CO)_5$	259(eq)	240(eq)	1.827(eq)[b]	239[f]
	236(ax)	180(ax)	1.807(ax)[b]	239[f]
$Co(CO)_4^-$	333	348	1.794[c]	400±20[f]
	NR	QR		
$Nb(CO)_6^-$	226	262	2.089[d]	319[g]
$Mo(CO)_6$	251	293	2.063[e]	344[f]
$Rh(CO)_4^-$	604	713	1.975[a]	778[f]
$W(CO)_6$	547	816	2.058[e]	997[f]

[a]Optimized geometry. [b]Reference 52. [c]Reference 53. [d]Reference 54.
[e]Reference 55. [f]Reference 37. [g]Reference 38. [h]In SI units of 10^{19} kg m^{-2} s^{-2} A^{-2}.

It follows from Eq. (2.25) that contributions to $K(M,C)_{ii}^{FC}$ come from pairs of one occupied orbital Φ_k^0 and one virtual orbital Φ_l^0. Further, appreciable contributions are only possible if Φ_k^0 and Φ_l^0 are non-zero on both nuclei. Thus, core orbitals are not going to add much to $K(M,C)_{ii}^{FC}$ as they are localized on one of the centers only.

It is possible to give a detailed analysis of the contribution to $K(M,C)_{ii}^{FC}$ from each pair of occupied and virtual orbitals. However, it will be more useful to divide $K(M,C)_{ii}^{FC}$ into contributions from one occupied and all virtual orbitals. Because of the unique symmetry of the delta function operator involved, such an analysis is meaningful for the FC coupling term but not for the PSO coupling term (see discussions below and section 2.4.2). For the same reason, there are only a few occupied orbitals in transition metal complexes that can give contributions (see discussions below).

This suggests the possibility of making qualitative predictions regarding the magnitude of $K(M,C)_{ii}^{FC}$ by looking at just a few MOs of the metal complexes. In the following we shall conduct such an analysis for the carbonyl systems and extend it to other metal complexes, including those dealt with in later sections.

For the metal center only atomic s-type orbitals have non-zero values at the nucleus. Furthermore, s-type orbitals on the metal span the totally symmetric representation, which implies that only occupied and virtual molecular orbitals from this representation will contribute significantly to $K(M,C)_{ii}^{FC}$. The totally symmetric valence orbitals Φ_k^0 and Φ_l^0 are made up of the *n*s and (*n*+1)s metal orbitals (*n*=3,4,5) and the ligand based orbitals $1\sigma_L$ and $2\sigma_L$, Figure 2.1. The ligand-based orbitals $1\sigma_L$ and $2\sigma_L$ are symmetry combinations of the highest occupied σ-orbitals, 4σ and 5σ, on each CO ligand. Here 4σ and 5σ are the only occupied CO orbitals with substantial contributions from 2s on carbon, Figure 2.2. The resulting molecular orbitals from the interaction between *n*s, (*n*+1)s and $1\sigma_L$, $2\sigma_L$ give rise to three occupied (1a, 2a and 3a) and one unoccupied (4a) orbitals, Figure 2.1. The actual composition of 2a and 3a is shown in Table 2.2 for the three 3d-complexes. We shall in the following refer to orbitals in the totally symmetric representation as *n*a (*n*=1,2,3) without subscripts applicable to the specific point groups.

The 1a level of lowest energy is represented by a *n*s based orbital (stabilized from above) with in-phase bonding contributions from $1\sigma_L$, $2\sigma_L$ and (*n*+1)s in accordance with general considerations based on perturbation theory. It is too low in energy to couple with the virtual orbitals on account of the factor $1/(\varepsilon_k^O - \varepsilon_l^O)$ of Eq. (2.25). We note that the virtual orbitals (including 4a) will all be destabilized (from below) with out-of-phase contributions from ns, $1\sigma_L$ and $2\sigma_L$, again in accordance with perturbation theory. Thus *n*s, $1\sigma_L$ and $2\sigma_L$ will be of the same phase in the unoccupied orbitals.

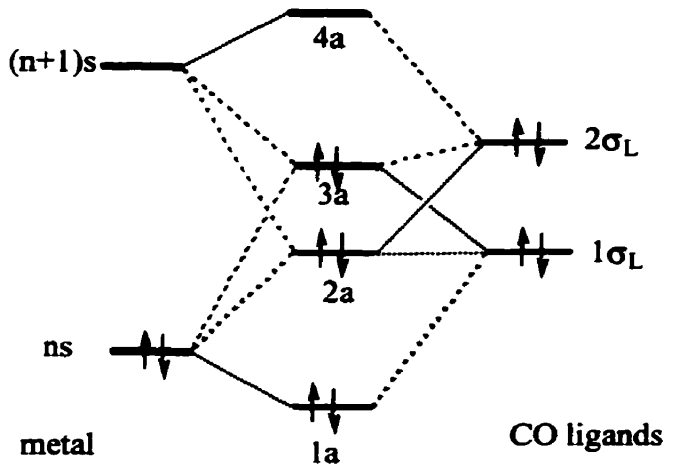

Figure 2.1 Interaction diagram for the MOs contributing to the FC coupling term in carbonyl complexes.

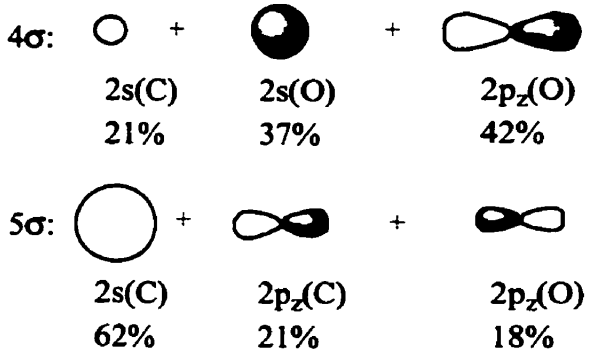

Figure 2.2 Composition of the carbonyl σ orbitals containing the carbon 2s AO.

The level 2a is $1\sigma_L$ based whereas 3a is dominated by $2\sigma_L$. Both are destabilized (from below) by out-of-phase contributions from *n*s and stabilized (from above) by in-phase contribution from (n+1)s and other s-type metal orbitals of even higher energy. In 2a the orbital $2\sigma_L$ will add (from above) in-phase so that the contributions to 2a from $1\sigma_L$ and $2\sigma_L$ are of the same sign. By contrast, $1\sigma_L$ will add (from below) out-of-phase to 3a with the result that the contributions to 3a from $1\sigma_L$ and $2\sigma_L$ are of different signs, Table 2.2.

Table 2.2 Molecular orbital expansion coefficients[i] in terms of metal and ligand fragment orbitals for 2a and 3a in some 3d-transition metal carbonyl complexes.

Fragment orbital	2a			3a		
	$V(CO)_6^-$	$Fe(CO)_5$	$Co(CO)_4^-$	$V(CO)_6^-$	$Fe(CO)_5$	$Co(CO)_4^-$
3s	-0.194	-0.184	-0.147	-0.170	-0.118	-0.155
4s	+0.002	+0.073	+0.032	+0.118	+0.092	+0.142
$1\sigma_L$	+0.840[a]	+0.43[c]	+0.871[g]	-0.524[a]	-0.449[c]	-0.476[g]
		+0.537[d]			-0.535[d]	
$2\sigma_L$	+0.337[b]	+0.311[e]	+0.312[h]	+0.721	+0.324[e]	+0.742[h]
		+0.353[f]			+0.512[f]	

[a] $1\sigma_L$ for $V(CO)_6^-$ is $1\sigma_L = 1/\sqrt{6}(4\sigma_1 + 4\sigma_2 + 4\sigma_3 + 4\sigma_4 + 4\sigma_5 + 4\sigma_6)$

[b] $2\sigma_L$ for $V(CO)_6^-$ is $2\sigma_L = 1/\sqrt{6}(5\sigma_1 + 5\sigma_2 + 5\sigma_3 + 5\sigma_4 + 5\sigma_5 + 5\sigma_6)$

[c] Equatorial component, $1\sigma_L^{eq}$, of $1\sigma_L$ in $Fe(CO)_5$, where
$1\sigma_L^{eq} = 1/\sqrt{3}(4\sigma_1^{eq} + 4\sigma_2^{eq} + 4\sigma_3^{eq})$

[d] Axial component, $1\sigma_L^{ax}$, of $1\sigma_L$ in $Fe(CO)_5$, where $1\sigma_L^{ax} = 1/\sqrt{2}(4\sigma_1^{ax} + 4\sigma_2^{ax})$

[e] Equatorial component, $2\sigma_L^{eq}$, of $2\sigma_L$ in $Fe(CO)_5$, where
$2\sigma_L^{eq} = 1/\sqrt{3}(5\sigma_1^{eq} + 5\sigma_2^{eq} + 5\sigma_3^{eq})$

[f] Axial component, $2\sigma_L^{ax}$, of $2\sigma_L$ in $Fe(CO)_5$, where $2\sigma_L^{ax} = 1/\sqrt{2}(5\sigma_1^{ax} + 5\sigma_2^{ax})$

[g] $1\sigma_L$ for $Co(CO)_4^-$ is $1\sigma_L = 1/2(4\sigma_1 + 4\sigma_2 + 4\sigma_3 + 4\sigma_4)$

[h] $2\sigma_L$ for $Co(CO)_4^-$ is $2\sigma_L = 1/2(5\sigma_1 + 5\sigma_2 + 5\sigma_3 + 5\sigma_4)$

[i] The coefficients listed are from the all-electron calculations.

Both 2a and 3a are of sufficiently high energy to couple with virtual orbitals and contribute to $K(M,C)_{ii}^{FC}$. We present in Table 2.3 the contributions to $K(M,C)_{ii}^{FC}$ from the couplings of 2a and 3a, respectively, with all virtual orbitals. It is not surprising that the contribution from 2a is large because $1\sigma_L$ and $2\sigma_L$ both enter with the same sign into that orbital, Tables 2.2 and 2.3. On the other hand, substantial cancellations will take place in the contributions from 3a where $1\sigma_L$ and $2\sigma_L$ enter with opposite signs. The contribution from 3a is as a consequence small and in some cases of opposite sign.

Table 2.3 Molecular orbital contributions[a] to $K(M,C)^{FC}$ with frozen-core and all-electron basis in some 3d-carbonyl complexes.

molecule	2a		3a		Total $K(M,C)^{FC}$	
	FRC	AE	FRC	AE	FRC	AE
$V(CO)_6^-$	123	100	41	26	162	133
$Fe(CO)_5$	195(eq)	194(eq)	-21(eq)	-17(eq)	267(eq)	248(eq)
	289(ax)	287(ax)	20 (ax)	27 (ax)	258(ax)	205(ax)
$Co(CO)_4^-$	221	247	80	96	333	348

[a]In SI units of 10^{19} kg m^{-2} s^{-2} A^{-2}.

The contributions to $K(M,C)_{ii}^{FC}$ will in general come from a few occupied ligand based orbitals of sufficiently high energy to couple with the virtuals. The magnitude, and even the sign, will depend from case to case on the nodal structure of the ligand-based orbitals. We shall now state a few more general observations in connection with the results presented in Table 2.1.

We note that $K(M,C)_{ii}^{FC}$ decreases along the 3d-series $Co(CO)_4^-$, $Fe(CO)_5$ and $V(CO)_6^-$ with increasing coordination number. A similar trend is found for the 4d-series, $Rh(CO)_4^-$, $Nb(CO)_6^-$. The trend is readily understood when we note that the contribution to 2a and 3a from $1\sigma_L$ and $2\sigma_L$ is roughly the same for all complexes, Table 2.2. However the contribution from 4σ and 5σ on any single ligand to $1\sigma_L$ and $2\sigma_L$ decreases as $1/\sqrt{n}$ with the coordination number n, Table 2.2. Thus the value of the 2a and 3a orbitals on any single carbon nucleus will diminish with increasing coordination number n. As a result $K(M,C)_{ii}^{FC}$ is seen to decrease through the series $Co(CO)_4^-$, $Fe(CO)_5$ and $V(CO)_6^-$, and $Rh(CO)_4^-$, $Nb(CO)_6^-$.

It follows from Table 2.1 that the coupling constants calculated by the nonrelativistic method (NR) are too small for the 4d- and 5d-transition metal carbonyls. The inclusion of relativistic effects (QR) brings the calculated values into better agreement with experiment by increasing the coupling constants from 20% for the 4d-complexes to 50% for the 5d-complexes. The major impact of relativity is to reduce the

kinetic energy of electrons passing at high instantaneous velocities near the nucleus[39-43]. The reduction in the destabilization from a high kinetic energy will enhance[39,41,42] the finite probability of finding *n*s and (*n*+1)s valence electron near the nucleus and thus increase $K(M,C)_{ii}^{FC}$. The reduction in kinetic energy will also result in a contraction of the chemical bond[39,41], which indirectly would increase $K(M,C)_{ii}^{FC}$. However, this effect is not included in the reported calculated differences between coupling constants obtained from nonrelativistic and quasirelativistic methods since both sets of calculations were carried out at the same geometry, Table 2.1. The quasi-relativistic method employed here is only applicable for valence orbitals and might suffer variational collapse if extensive basis sets are employed near the nucleus[19-22]. We hope later to remove these deficiencies by resorting to a more refined relativistic treatment[44-47]. Such a treatment should also improve on the coupling constants calculated for the 4d-, and especially, 5d-complexes.

We shall finally comment on the influence of the frozen-core approximation. Our analysis of the results from all-electron calculations clearly indicates that the contribution to $K(M,C)_{ii}^{FC}$ of Eq. (2.25) from occupied core orbitals, in the summation over *k*, is completely negligible. This is so because the core orbitals are localized on one center and too low in energy to couple with the virtuals. Thus, as mentioned before, only couplings between the occupied 2a and 3a valence orbitals and the virtuals are of importance. These couplings are nevertheless influenced indirectly by the core description, Table 2.3. As the core is unfrozen in the all-electron zeroth order molecular calculation, the core orbitals will relax in comparison to the atomic state. This relaxation will in turn influence the composition of valence orbitals such as 2a and 3a, and modify the calculated coupling constant $K(M,C)_{ii}^{FC}$.

2.3.2 Transition-metal oxo complexes

Table 2.4 summarizes our calculated nuclear coupling constants in 3d- and 4d-transition metal oxo complexes. The Fermi-contact and paramagnetic spin-orbit contributions are listed separately. Again we compare frozen-core and all-electron results for 3d-complexes and nonrelativistic frozen-core calculations and relativistic frozen-core calculations for 4d-complexes. It is clear that the all-electron results for 3d-complexes are in good agreement with experiment (except for MnO_4^-), while both nonrelativistic and quasi-relativistic calculations give values that are 10% lower than the experimental estimates for the 4d-complexes.

Table 2.4 Reduced coupling constants[g] K(M-O) in some 3d-, 4d- and 5d-transition-metal oxo complexes.

molecule	r_{M-O}	K(M-O)^{FC}		K(M-O)^{PSO}		K(M-O)		K^{Expf}
		FRC	AE	FRC	AE	FRC	AE	
VO_4^{3-}	1.711[a]	289	243	-93	-94	197	150	144
CrO_4^{2-}	1.653[b]	276	244	-140	-140	135	104	108
MnO_4^-	1.629[c]	225	218	-190	-189	36	29	75
		NR	QR	NR	QR	NR	QR	
MoO_4^{2-}	1.765[d]	479	464	-123	-118	355	346	380
TcO_4^-	1.676[e]	537	531	-132	-128	408	403	359

[a]Reference 56. [b]Reference 57. [c]Reference 58. [d]Reference 59. [e]Reference 60. [f]Reference 61. [g]In SI units of 10^{19} kg m^{-2} s^{-2} A^{-2}.

We shall first discuss the FC coupling term in the oxo-complexes using the concepts introduced in the last section. In the tetroxo complexes, $1\sigma_L$ and $2\sigma_L$ of Figure 2.1 are represented by 2s(O) and 2p(O), respectively. The 2a orbital is an out-of-phase combination of metal ns and 2s(O) with nearly equal contributions as 2s(O) is close in energy to *n*s. Thus, the contribution to $K(M,O)^{FC}$ from the coupling of 2a with all virtual orbitals in oxo complexes, Table 2.5, is expected to be larger than in the carbonyl complexes, Table 2.3, where 2a is made up mostly of carbonyl sigma orbitals of much higher energy than 2s(O). The 3a orbital consists of in-phase (*n*+1)s and 2p(O) components with an in-phase contribution from 2s(O). As 2s(O) enters with different signs relative to the leading s-component in 2a and 3a, respectively, the latter orbitals will have contributions of different signs to $K(M,O)^{FC}$, Table 2.5. Further, it follows from Table 2.5 that the contribution from 2a and 3a increases across the first transition metal series from VO_4^{3-} to MnO_4^- in absolute terms. This can be explained again by the increase in the covalent character of both 2a and 3a. The total $K(M,O)^{FC}$, however, hardly changes, because 2a and 3a contributions have different signs.

Table 2.5 Molecular orbital contributions[a] to $K(M\text{-}O)^{FC}$ from frozen-core and all-electron calculations in some 3d-transition-metal tetroxo complexes.

molecule	2a		3a		Others	
	FRC	AE	FRC	AE	FRC	AE
VO_4^{3-}	453	408	-138	-137	-26	-28
CrO_4^{2-}	487	440	-190	-175	-21	-21
MnO_4^-	497	457	-250	-229	-22	-10

[a]In SI units of 10^{19} kg m^{-2} s^{-2} A^{-2}.

The PSO coupling term of Eq. (2.20) can be written in a compact form as

$$K(A,B)_{ii}^{PSO} = -2\left(\frac{\mu_o \beta}{2\pi}\right)^2 \sum_k^{occ} \sum_l^{vir} \frac{\int \Phi_l^o \hat{M}_i^A \Phi_k^o d\bar{r}_A \int \Phi_l^o \hat{M}_i^B \Phi_k^o d\bar{r}_B}{\varepsilon_k^o - \varepsilon_l^o}. \qquad (2.26)$$

In contrast to the carbonyls, $K(A,B)_{ii}^{PSO}$ is seen to be important for the oxo systems. It can numerically be of the same magnitude as the FC coupling term, but is of opposite sign, Table 2.4. The diagonal terms $K(A,B)_{ii}^{PSO}$ (i=x,y,z) are all equal for the orientation shown in Figure 2.3. Thus, each of the components will represent the PSO contribution, $K(A,B)_{ii}^{PSO}$, to the reduced coupling constant of Eq. (2.4).

The magnetic operator $\hat{M}_i^G = (\bar{r}_G \times \bar{\nabla})_i / r_G^3 = iL_i^G / r_G^3$ of Eq. (2.26) is effectively localized on one center G=A,B, due to the $1/r_G^3$ dependence. It is thus clear that the occupied, Φ_k^0, and virtual, Φ_l^0, orbitals must have contributions on both metal (G=A) and ligand (G=B) atomic orbitals in order for the product of the two integrals in Eq. (2.26) to be nonvanishing. We shall refer to this as the polarization factor. Also, it is evident that $K(A,B)_{ii}^{PSO}$ is determined by couplings from the frontier occupied and virtual orbital pairs due to the inverse energy dependence $1/(\varepsilon_k^0 - \varepsilon_l^0)$. The effect of the rotational operator $\hat{L}_i^G$ on p and d orbitals has been tabulated in the literature[48].

In Table 2.6 we present the significant contributions to K(M,O)^{PSO} from the occupied-virtual frontier orbital pairs in the case of the 3d-transition metal tetroxo complexes. Because our calculations reveal that the PSO coupling term is insensitive to the size of basis set and the inclusion of the core electrons, we only show the results from all-electron calculations. The molecular frontier orbitals are linear combinations[49] of metal based d-components and p-type oxygen orbitals that can be characterized as either of σ or π symmetry, Figure 2.3. We present their composition in Table 2.7.

It follows from Table 2.6 that ^1K(M,O)^{PSO} can be attributed mainly to the couplings between the occupied orbitals of highest energy $5t_2$, $6t_2$ and the virtual orbitals $7t_2^*$, $2e^*$ of lowest energy[49]. Here $5t_2$, $6t_2$ and $7t_2^*$ represents the bonding (between metal d and oxygen p orbitals), non-bonding (oxygen lone pair p orbitals) and anti-bonding orbitals of t_2-symmetry, respectively, whereas $2e^*$ is anti-bonding with respect to metal d and oxygen π-orbitals, Table 2.7. Due to the relative energies of the metal and oxygen AOs, the occupied orbitals are polarized toward oxygen and the virtual ones are polarized toward metal. For all three complexes, the coupling $5t_2$-$7t_2^*$ gives the largest contribution,

whereas the smaller contributions from $5t_2$-$2e^*$ and $6t_2$-$7t_2^*$ couplings are of approximately the same magnitude but of opposite sign. An additional small contribution comes from the $6t_2$-$2e^*$ coupling.

Table 2.6 Molecular orbital contributions[a] to $K(M\text{-}O)^{PSO}$ in some 3d-transition-metal tetroxo complexes.

	VO_4^{3-}		CrO_4^{2-}		MnO_4^-	
	ΔE(e.v.)	K^{PSO}	ΔE(e.v.)	K^{PSO}	ΔE(e.v.)	K^{PSO}
$5t_2$-$7t_2^*$	8.154	-57	8.021	-83	7.673	-112
$5t_2$-$2e^*$	6.836	-26	6.405	-45	6.003	-71
$6t_2$-$7t_2^*$	6.763	29	6.144	47	5.337	66
$6t_2$-$2e^*$	5.445	-15	4.528	-18	3.667	-14

[a]In SI units of 10^{19} kg m^{-2} s^{-2} A^{-2}.

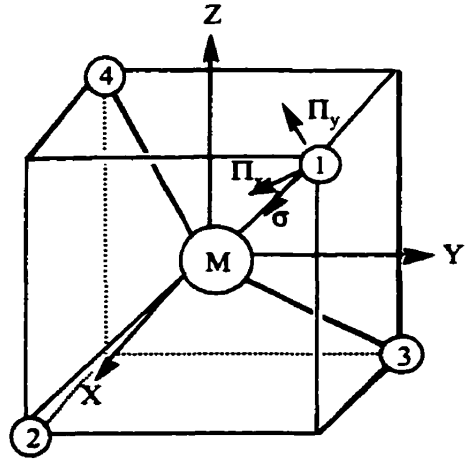

Figure 2.3 The orientation of the ligand O_1 orbital in a tetroxo complex.

The direction cosines are: $\sigma : \frac{1}{\sqrt{3}}(-1,-1,-1); \pi_x : \frac{1}{\sqrt{3}}(1,-1,0); \pi_y : \frac{1}{\sqrt{3}}(-1,-1,2).$

Table 2.7 Molecular orbital coefficients[a,b,c] in the frontier orbitals of CrO_4^{2-}.

	$5t_{2y}$	$6t_{2y}$	$7t_{2z}$*	$2e_x$*	$2e_y$*
d_{xz}(M)	0.531	0.027			
d_{xy}(M)			0.881		
d_{z2}(M)				0.866	
d_{x2-y2} (M)					0.866
σ'	0.324	0.280	-0.338	0.004	0
π_x'	0.161	-0.330	0	0	-0.361
π_y'	0.093	-0.190	0.244	-0.360	0

[a]The detailed composition of the molecular orbital of d^0 tetroxo complexes has been discussed in Reference 49 . [b]The coordinate system for CrO_4^{2-} and the definition of the oxygen σ, π_x and π_y orbitals on any single center are given in Figure 2.2. [c]The σ', π_x' and π_y' orbitals are linear symmetry combinations of the σ, π_x and π_y orbitals from each oxygen center. They are defined in Reference 49.

For the *x*-component, $K(A,B)_{xx}^{PSO}$, the operator $\hat{M}_x^G$ will couple t_{2y} with t_{2z} and t_{2x} with e_a, e_b through rotations[48] by $\hat{L}_x^G$ of respectively the d-based metal orbitals and the p-type oxygen orbitals of σ and π symmetry, Table 2.7. As the most important contributions, we consider the coupling of $5t_2$ and $6t_2$ with $7t_2$ and $2e_{a,b}$, respectively. It follows from Table 2.7, that $5t_{2y}$ has large coefficients on both metal d_{xz} and oxygen σ and π_x orbitals whereas $6t_{2y}$ is mainly a nonbonding orbital with large coefficients on oxygen σ, π_x and π_y orbitals, only. It is thus clear why $5t_2$ is better able to couple with the virtual orbitals although it is of lower energy, Table 2.6. On the metal center, a rotation about the x axis will bring d_{xy}(M) in $7t_{2z}^*$ to d_{xz}(M) so that it can overlap with the same orbital in $5t_{2y}$, while on the ligand center σ and π_y orbitals in $7t_{2z}^*$ are rotated about the same axis to σ, π_x and π_y, which then overlap with the same orbitals in $5t_{2y}$.

In the same way, both $2e_a^*$ and $2e_b^*$ can couple with $5t_{2x}$ through the rotation about the x axis. However, the contributions from $2e_a^*$ and $2e_b^*$ are of opposite signs, which makes the contribution from the $5t_2$-$2e^*$ coupling smaller than what one might expect from relative energies and orbital compositions, Table 2.6 and 2.7.

Across the series VO_4^{3-}, CrO_4^{2-} and MnO_4^-, the contributions from the three most important couplings are seen to increase in absolute terms, Table 2.6. This is due to a decrease in the energy gaps between occupied and virtual orbitals across the series, Table 2.6, as well as the increasing covalent character of both occupied and virtual MOs. Here the energy and the bond polarization criteria work in the same direction to increase $K(\mathrm{M,O})^{\mathrm{PSO}}$. For the 4d-oxo complexes we have carried out both nonrelativistic and quasirelativistic calculations. Relativistic corrections are seen to be minor for PSO and FC contributions, and the calculated coupling constants are in good agreement with experiment, Table 2.4.

The dominance of the polarization factor makes the interpretation of PSO coupling tensors in terms of MO-MO contributions different from the interpretation of the related paramagnetic (spin-orbit) shielding tensors[50]. In the common-gauge-origin DFT formulation[1], the paramagnetic shielding on nucleus G can be expressed as

$$\sigma(G)_{ii}^{P} \approx -\left(\frac{\mu_0 e^2 c}{4\pi\hbar}\right)^2 \sum_{k}^{occ}\sum_{l}^{vir} \frac{\int \Phi_l^o \hat{M}_i^G \Phi_k^o d\bar{r}_G \int \Phi_l^o i\hat{L}_i \Phi_k^o d\bar{r}_G}{\varepsilon_k^0 - \varepsilon_l^0}. \qquad (2.27)$$

Here, the local magnetic operator is present only in the first integral, whereas in the second integral the rotational operator has contributions from all centers. Accordingly, orbitals localized on G would give a very large contribution to the paramagnetic shielding. This is why the lone pair orbital $6t_2$ plays an important role in the ^{17}O shielding[50] but not in the PSO M-O coupling, as it is only localized on one nucleus. Also, the important magnetic dipole transitions, which give significant contributions to ^{17}O NMR shielding, are not of importance in nuclear M-O couplings. In fact, the strong magnetic dipole transition $1t_1$-$2e^*$ contributes considerably to the ^{17}O paramagnetic shielding in the tetroxo complexes[50], but gives only negligible contribution to the M-O PSO coupling term.

Compared with experiment, the exceptionally large discrepancy of the calculated coupling constant in MnO_4^- could be related to the error in the present DFT formulation of the PSO coupling term due to the neglect of current density, Eq. (2.13). A large disagreement was also found in the NMR shielding calculation of MnO_4^- where the same approximation was invoked.[50,51] Another source of error might be the FC term.

2.3.3 Transition-metal hexafluoro complexes

The nuclear spin-spin coupling in transition metal d^0 fluoro complexes can be analyzed in a way similar to that of the coupling in d^0 oxo complexes. We present in Table 2.8 our calculated K(M,F) coupling constants for some transition-metal hexa fluoro complexes. The nonrelativistic frozen-core results are given for the 3d-complexes while results for the 4d- and 5d-complexes are based on both of the non- and quasirelativistic methods. An extended basis set was required on the fluorine atom in order to converge the calculated FC coupling constants. A similar extended basis was required for an accurate determination of FC coupling terms in the fluorinated main-group compounds[2]. It can be seen from Table 2.8 that the FC and PSO terms are of equal importance for nuclear couplings in the fluoro complexes. In some cases, for example VF_6^-, the PSO contribution is even larger than the FC contribution. The calculated values are in general lower in absolute terms than the experimental estimates, especially for the 3d-complex ScF_6^{3-} and the 4d-complex NbF_6^-.

Table 2.8 Reduced coupling constants[h] K(M-F) in some 3d-, 4d- and 5d-transition-metal hexafluoro complexes.

molecu	r_{M-O} (Å)	K(M-F)^{FC}		K(M-F)^{PSO}		K(M-F)		$K^{exp.}$
ScF_6^{3-}	2.035[a]	77		-30		49		59.6[f]
TiF_6^{2-}	1.856[b]	114		-63		51		53.2[f]
VF_6^-	1.817[c]	91		-118		-27		29.7[f]
		NR	QR	NR	QR	NR	QR	
NbF_6^-	1.886[d]	216	190	-123	-120	96	74	125[f]
WF_6	1.780[e]	558	381	-305	-304	260	84	86.6[g]

[a]Reference 62. [b]Reference 63. [c]Optimized geometry. [d]Reference 64. [e]Reference 44. [f]Reference 65. [g]Reference 66. [h]In SI units of 10^{19} kg m^{-2} s^{-2} A^{-2}. Results are from the frozen-core calculations.

The d^0 transition-metal fluoro complexes have two valence type orbitals, 2a and 3a, contributing to the FC term. The 2a orbital of lower energy is an out-of-phase combination between *n*s on the metal and 2s(F), Figure 2.1. The 3a orbital is 2p(F) based with in-phase contributions from (*n*+1)s(M) and 2s(F). The composition and phases of both orbitals are analogous to the oxo systems and readily understood from considerations based on perturbation theory, Section 2.3.1.

The fluoro complexes have in general smaller FC contributions than their oxo analogies. For instance, the 2a contribution to the FC coupling is 231 in VF_6^-, compared with 453 in VO_4^{3-}, Tables 2.5 and 2.9. This can be attributed mainly to the higher coordination number. The higher coordination number results in a smaller coefficient on the AO's in 2a and 3a from the fluorine ligand under consideration, Section 2.3.1. We note further that the FC contributions from 2a and 3a are of opposite sign in analogy with the carbonyls and the oxo complexes. The origin of the sign changes is simply that 2s(F) and the leading metal s-contribution is out of phase in 2a and in phase in 3a. Further, 2a contributes more in absolute terms as it has the larger 2s(F) component. From Table 2.8,

we find no obvious trend for the FC contributions across the periodic series ScF_6^{3-}, TiF_6^{2-} and VF_6^-. Down a periodic triad VF_6^- and NbF_6^-, however, the FC coupling is increasing because of the greater value of the *n*s and (*n*+1)s orbitals on the nucleus for the heavier element.

Table 2.9 Molecular orbital contributions[a] to $K(M\text{-}F)^{FC}$ in some 3d- and 4d-transition-metal hexa fluoro complexes.

molecule	2a		3a		Others	
ScF_6^{3-}	128		-47		-4	
TiF_6^{2-}	219		-97		-8	
VF_6^-	231		-140		0	
	NR	QR	NR	QR	NR	QR
NbF_6^-	468	508	-233	-294	-19	-24
WF_6	1165	1491	-496	-1035	-111	-72

[a]In SI units of 10^{19} kg m^{-2} s^{-2} A^{-2}.

In the transtion-metal carbonyl systems, we have seen that relativity significantly increases the magnitude of $K(M,F)^{FC}$, especially in the 5d-complexes. However, for the fluoro complexes, Table 2.8, the quasirelativistic calculations on the FC coupling term exhibit smaller values than the nonrelativistic ones. As mentioned before, the relativistic enhancement of the electron density at the nucleus increases both the 2a and 3a contribution to the FC term. Consequently, in the case of both contributions having the same sign, the magnitude of $K(M,F)^{FC}$ increases. On the other hand, in the case of two contributions having opposite sign, the $K(M,F)^{FC}$ value will decrease if the magnitude of the increase in the negative contribution is larger. This is the reason why relativistic effects reduce the FC term in both NbF_6^- and WF_6 complexes, Table 2.9, and also in the 4d-transition metal oxo complexes, Table 2.4. Since the FC term in NbF_6^- is the same order of magnitude as the PSO term, the relativistic correction with respect to the total

coupling constant in NbF_6^- is seen to be much larger than in the 4d-transition-metal oxo complexes, Table 2.4 and Table 2.8. The large underestimation of the coupling value in NbF_6^- is in accordance with our calculations in the oxo complexes. Finally, it is also observed that in contrast to the FC term, scalar relativity seems to have much smaller influence on the PSO term, Table 2.4 and Table 2.8.

As discussed in Section 2.3.2, the main contributions to $K(M,F)^{PSO}$ come from the couplings between metal-ligand bonding and anti-bonding frontier orbitals with both metal d- and ligand σ or π components. In the hexafluoro complexes, $3e_g$ and $1t_{2g}$ represent the occupied ligand-metal bonding orbitals of respectively σ– and π– symmetry with $1t_{2g}$ of highest energy. Furthermore, $4e_g^*$ and $2t_{2g}^*$ are the corresponding empty anti-bonding orbitals with $2t_{2g}^*$ of lowest energy.

Figure 2.4 illustrates the couplings of occupied and virtual orbitals in the evaluation of $K(M,F_1)^{PSO}$, where F_1 lies along the positive y-axis. There are two equivalent contributions to $K(M,F_1)^{PSO}$ from the components of $K(M,F_1)_{ii}^{PSO}$ $(i=x,z)$ perpendicular to the M-F_1 bond axis as well as one unique contribution, $K(M,F_1)_{ii}^{PSO}$, from the direction along the M-F_1 bond axis. For $i=x,z$ the operators $\hat{L}_i$ $(i=x,z)$ rotate $d(M)_\pi$ into $d(M)_\sigma$ and $p(F)_\pi$ into $p(F)_\sigma$, thus orbitals t_{2g} couples with e_g, Figure 2.4a. For $i=y$ the $\hat{L}_y$ operator rotates one set of $d(M)_\pi$ and $p(F)_\pi$ components into another, thus two different t_{2g} components couple with each other, Figure 2.4b.

The $3e_g(\sigma)$-$2t_{2g}^*(\pi^*)$ and $1t_{2g}(\pi)$-$2t_{2g}^*$ (π^*) pairs of occupied and virtual orbitals have the smallest energy gaps, Table 2.10, and afford in all cases principal contributions to $K(M,F_1)^{PSO}$, with $3e_g(\sigma)$-$2t_{2g}^*(\pi^*)$ being more important as it has two contributions from the components perpendicular to the M-F bond. Another pair of importance is $1t_{2g}(\pi)$-$4e_g^*(\sigma^*)$ with a larger energy gap. The periodic trend in $K(M,F)^{PSO}$ for the 3d-transition metal fluoro complexes is readily understood in terms of the change in the energy gap between occupied and virtual orbitals as well as the degree of covalency, Table 2.8 and Table 2.10.

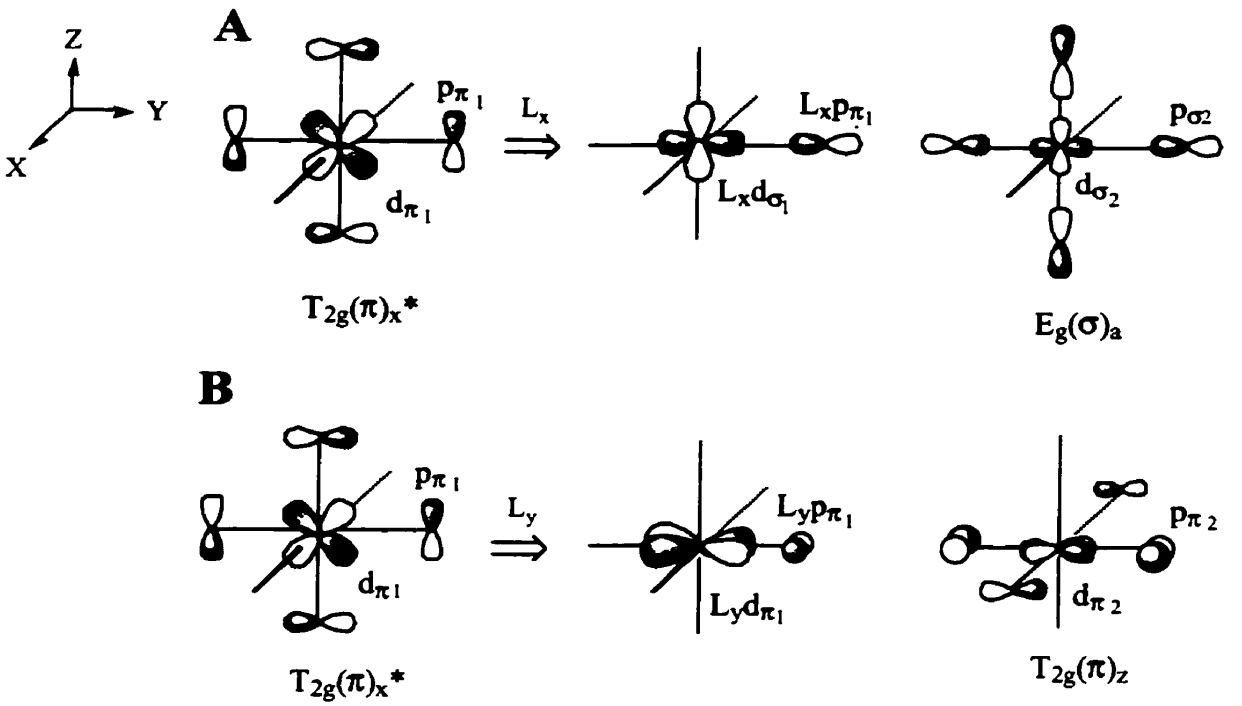

Figure 2.4 PSO coupling in octahedral complexes.

Table 2.10 Molecular orbital contributions to $K(\text{M-F})^{\text{PSO}}$ in some 3d-transition-metal fluoro complexes.

	ScF_6^{3-}		TiF_6^{2-}		VF_6^-	
	ΔE(e.v.)	K^{PSO}	ΔE(e.v.)	K^{PSO}	ΔE(e.v.)	K^{PSO}
$3e_g(\sigma)$-$2t_{2g}^*(\pi^*)$	8.603	-15	7.829	-37	6.381	-84
$1t_{2g}(\pi)$-$2t_{2g}^*(\pi^*)$	8.291	5	7.365	14	5.719	36
$1t_{2g}(\pi)$-$4e_g^*(\sigma)$	7.563	-1	9.589	-10	8.508	-57
$1t_{2g}(\pi)$-$5e_g^*(\sigma)$	10.599	-11	10.943	-16	13.377	-3
Others		-8		-14		-10

[a]In SI units of 10^{19} kg m^{-2} s^{-2} A^{-2}.

2.3.4 Transition-metal trifluorophosphine complexes

Our calculations of metal-phosphorus coupling constants in 3d- and 4d- transition-metal trifluorophosphine complexes show generally good agreement with experiment. The results from calculations in which the core was frozen on the metal center are presented in Table 2.11. Unlike the calculations shown before, we observe no systematic trend in the errors for the 3d-complexes. However, the absolute deviation from the experimental values is overall about 17%. Since nuclear coupling constants are very sensitive to geometrical changes, one might ascribe part of the error to the inaccuracy in the geometry optimizations. Comparing theoretical coupling constants in the 4d-transition metal phosphine complexes with experiment, one can see that the nonrelativistic method gives 10% lower values and the quasirelativistic method gives 10% higher values. Finally, it is not surprising to see that the extraordinary large coupling in the 5d-complex $Pt(PF_3)_4$ is only partly reproduced (60 %) by our quasi-relativistic calculation.

Table 2.11 Reduced coupling constants[f] K(M-P) in some 3d-, 4d- and 5d-transition-metal trifluorophosphine complexes.

molecule	r_{M-P} (Å)	K(M-P)		$K^{Exp.}$
$V(PF_3)_6^-$	2.310[a]	466		399[c]
$Cr(PF_3)_6$	2.276[a]	460		386[d]
$Co(PF_3)_4^-$	2.076[a]	861		1063[c]
$Ni(PF_3)_4$	2.116[b]	903		1080[c]
		NR	QR	
$Nb(PF_3)_6^-$	2.474[a]	798	978	883[c]
$Mo(PF_3)_6$	2.425[a]	780	948	879[e]
$Pt(PF_3)_4$	2.230[b]	2981	3770	6215[c]

[a]Optimized geometry. [b]Reference 67. [C]Reference 68. [D]Reference 69. [E]Reference 70. [f]In SI units of 10^{19} kg m^{-2} s^{-2} A^{-2}.

The PSO contribution to the K(M,P) coupling constant in the phosphine complexes was found to be negligible. Thus, as in the carbonyls the calculated coupling constants can be analyzed and understood solely in terms of the FC contribution. We note further that the ratio between the metal-phosphorus coupling in phosphine complexes and the metal-carbon coupling in the corresponding carbonyls with the same metal center is larger than one and nearly constant. The stronger coupling in the phosphine complexes is due to the larger value in absolute terms of the 3s(P) orbital on the phosphorus nucleus compared to the absolute value of 2s(C) on the carbon nucleus.

The PF_3 ligand has three σ-type orbitals with contributions from 3s(P), Figure 2.5, for which the importance of the phosphorus 3s atomic orbital is in the order: $4\sigma_L > 2\sigma_L > 3\sigma_L$. The interaction between these orbitals and the two s-based metal orbitals, Figure 2.6, will give rise to four totally symmetric occupied orbitals. The 1a orbital is too low in energy and too polarized toward metal ns to contribute to the FC component of the coupling constant. The orbitals 2a, 3a, and 4a have major contribution from $2\sigma_L$, $3\sigma_L$, and $4\sigma_L$, respectively, as well as ns and (n+1)s. Given the composition of 2a, 3a, and 4a in terms of $2\sigma_L$, $3\sigma_L$, and $4\sigma_L$, as well as the relative occurence of 3s(P) in the σ-type orbitals, one can understand why the contributions from the na orbitals to the FC component of the coupling constant come in the order 4a>2a>3a, Table 2.12.

Table 2.12 Molecular orbital contributions[a] to $K(\text{Ni-P})^{FC}$ in $Ni(PF_3)_4$.

Orbital	2a	3a	4a	Others
K^{FC}	325	147	476	-37

[a]In SI units of 10^{19} kg m^{-2} s^{-2} A^{-2}.

The trends observed experimentally for the K(M,P) coupling constants across a series and down a triad for the 3d- and 4d-complexes are well reproduced by our calculations although there are deviations between experimental and theoretical values. As in the case of the carbonyls, quasi-relativistic calculations on the 4d-phosphine complexes are seen to increase the FC coupling constant compared to the nonrelativistic estimates as the values of the ns and (n+1)s orbitals on the metal center are increased in absolute terms. Even the quasirelativistic calculation on the 5d-complex $Pt(PF_3)_4$ fails to account for the large K(M,P) coupling constant. Here a better relativistic treatment will be required.

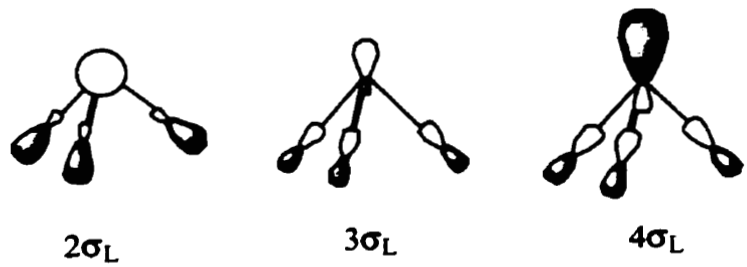

Figure 2.5 Composition of the trifluorophosphine ligand orbitals containing the phosphorus 3s AO.

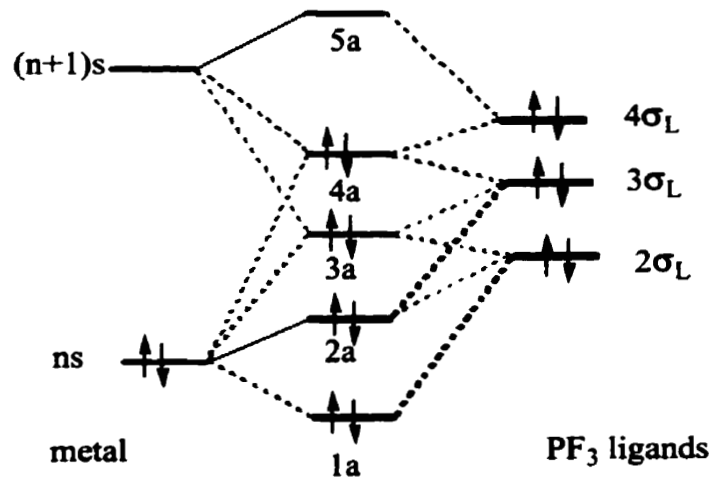

Figure 2.6 Interaction diagram for the MOs contributing to the FC coupling in trifluorophosphine complexes.

2.4 Concluding remarks

A newly implemented DFT based scheme for the calculation of nuclear magnetic resonance spin-spin coupling constants has been applied to the study of various transition-metal systems of affordable size, for which experimental coupling constants are available. We have presented results for metal-ligand one-bond couplings ^1K(M,X), in 3d-, 4d- and 5d-transition-metal carbonyl, oxo, fluoro, and phosphine complexes.

The two major contributions to the metal-ligand coupling constant come from the Fermi- contact term (FC) and the paramagnetic spin-orbit term (PSO). The FC contribution was evaluated by finite perturbation theory and the PSO part by an uncoupled perturbation approach. The finite perturbation theory, Eq. (2.22), was found to be numerically stable provided that the ligand is used as the perturbing atom. The uncoupled PSO approach, Eq. (2.20), in which any influence of the current density on the exchange correlation energy is neglected (see Eq. 2.13), performs well with the notable exception of MnO_4^-.

The results of the calculations on 3d- and 4d- complexes with frozen-core basis sets are (for the most part) in good agreement with experimental data and thus confirm the promising applicability of the current methodology. Using the quasirelativistic correction on top of the frozen- core treatment, the results on 5d-complexes are significantly improved. However, a more elaborate relativistic model is required to describe the nuclear region more accurately and bring the calculated results closer to experiment.

Contributions to ^1K(M,X) from FC were analyzed in terms of couplings between one occupied and all virtual molecular orbitals based on Eq. (2.25). Only molecular orbitals with contributions from s-type orbitals on ***both*** the ligand ***and*** the metal center contributes to $^1K(\text{M-X})^{FC}$. This precludes core orbitals and valence orbitals other than those in the totally symmetrical representation. Thus, the FC term can be viewed as a valence property, which allows the adoption of the frozen-core approximation for the calculation of systems containing heavy atoms. Furthermore, the contributions from the totally symmetrical representation involves the coupling of a few occupied valence orbitals (2-3) with the virtuals above.

The occupied valence orbitals are linear combinations of ns, $(n+1)$s on the metal and ns_L on the ligand. The sign of the contributions depends on the phases of the participating ns, $(n+1)$s and ns_L orbitals and can vary. The absolute magnitude decreases as the contributing orbital is polarized towards the ligand or the metal. Relativity enhances the contributions in absolute terms as the density of the ns and $(n+1)$s orbitals on the metal is increased. However, this might not result in a total increase in $^1K(\text{M-X})^{FC}$ due to the different signs of the individual contributions.

A similar analysis in terms of couplings between occupied and virtual orbitals has been carried out for the PSO term, Eq. (2.26). Again, only valence orbitals with contributions on ***both*** the metal ***and*** the ligand contribute. Thus core and lone-pair orbitals are not important. Using the MO based approaches, we have analyzed and rationalized trends in the calculated FC and PSO contributions to $^1K(\text{M,X})$ of 3d-, 4d- and 5d-transition metal-carbon, -oxygen, -fluorine and -phosphorus couplings.

Chapter 3

Scalar Relativistic Corrections to the Nuclear Spin-Spin Couplings

3.1 Introduction

The rapid development of high-speed computing resources and the recent advances in *ab initio* and Density functional theory (DFT) have enabled the theoretical prediction and interpretations of NMR chemical shifts and indirect spin-spin coupling constants. Since NMR parameters are used extensively by experimental chemists to identify and probe the structure of inorganic and organic compounds, the importance of their theoretical study cannot be overestimated. Over the last few years, a large number of papers has been published on calculations of NMR chemical shifts or shieldings. The interested reader may refer to the recent review articles by Helgaker[71] and Jameson[72]. In contrast, the theoretical aspects of nuclear spin-spin couplings have not yet attracted as much attention. So far, approaches based on the traditional ab initio methods such as CCSD[73,74], MCSCF[75], and MP2[76] have been developed. Due to the high computational demand of these methods, the applications are however restricted to selected diatomic molecules, second-row hydrides and a few small organic molecules[71]. More recently, the implementations in the DFT framework were reported by Malkin et al.[77] as well as by Dickson and Ziegler[2]. The latter implementation was later applied by us[78] to the study of nuclear spin-spin couplings in a series of transition-metal complexes. This work has demonstrated the ability of the currently used nonrelativistic DFT-based techniques to provide quantitative predictions of the coupling constants between 3d transition metals and directly bonded ligand atoms such as carbon, oxygen, fluorine and phosphorus. The fact that the nuclear spin-spin interactions involving oxygen and fluorine are less well described by the present methodology can be attributed to the deficiency of the existing exchange-correlation functionals in dealing with large electron correlations[79] and to the lack of the current dependency[80]. Further, the comparison of the nonrelativistic

predictions with experimental coupling values for 5d-transition-metal systems in this work[78] suggested that relativistic treatment is required for a quantitative description.

The study of relativistic effects on the indirect nuclear spin-spin coupling has rarely been attempted in the literature. In the seventies, Pyykkö et al. introduced a multiplicative "hydrogen-like" relativistic correction factor, originating from Breit[81], to account for the relativistic effects in Fermi-contact contribution to the nuclear couplings[82-84]. Later, Pyykkö developed a relativistic analogue[85] of Ramsey's spin-spin coupling expression[7], which in the early eighties was incorporated into the semi-empirical relativistic extended Hückel (REX) method[86]. With this approach, Pyykkö and Wiesenfeld calculated one-bond couplings in some small main-group compounds. The relativistic increase in ^1J(M-H) and ^1J(X-C) was found to be approximately 30% for SnH_4 and $Sn(CH_3)_4$, as well as more than 125% for the analogous lead compounds. They also found that the relativistic isotropic coupling constant is dominated invariably by the term, which has the nonrelativistic Fermi-contact (FC) origin. Recently, Kirpekar et al.[88] has applied the MCSCF method to investigate spin-orbit effects on the coupling constants in XH_4. The spin-orbit contribution to ^1J(M-H) was shown to be very small, amounting to about 1% for SnH_4. The findings by Pyykkö and Kirpekar et al. imply that the relativistic alteration of the coupling constant may be recovered by a scalar relativistic correction to the FC term without resorting to the two- or four-component relativistic coupling formalism. In the present work, we shall follow this idea and develop some simple relativistic correction schemes to account for the relativistic effects on the metal-ligand coupling constant.

In Ramsey's nonrelativistic nuclear spin-spin coupling theory[7], there are four terms contributing to the indirect nuclear spin-spin coupling constant: the Fermi contact and spin dipolar (SD) terms arising from the spin of the electron, and the para- and diamagnetic spin-orbit terms originating from the orbital motion of the electron. The FC operator takes effect whenever there is a finite electron density (s orbitals) at one nucleus and creates a net spin density (in a closed-shell molecule), which then interacts with the magnetic dipole of the second nucleus. The FC term gives in most cases the dominant contribution and is particularly sensitive to relativistic effects as a result of the orbital and

bond length contractions. Bond length shortening can be taken into account by making use of experimental geometries in the calculation. In the present paper, the remaining relativistic effects on the FC term can be accounted for to a first approximation by the following two approaches based on the nonrelativistic coupling formalism. The first approach involves the quasi-relativistic Pauli Hamiltonian[19,20,89,22] and is a straightforward analogue to the nonrelativistic method. The second scheme treats the effect of (s) orbital contraction on the FC term explicitly by replacing s orbitals in the self-consistent nonrelativistic Kohn-Sham orbitals by the relativistic ones without changing orbital expansion coefficients. We will describe in detail these two relativistic correction schemes in section 3.2. In section 3.3.1, we will test these schemes by calculating the metal-ligand coupling constants ^{1}J(M-L) in a series of group 12 and group 14 alkyl, cyano and hydrido complexes. In section 3.3.2, we will further validate the relativistic correction schemes on couplings involving a platinum atom, and examine the connection between *trans* influence and spin-spin couplings.

3.2 Computational Method and Details

3.2.1 The Quasi-Relativistic Kohn-Sham Method

Perhaps one of the most successful approaches to include relativity due to the first-order ($1/c^2$) relativistic operators is the frozen-core based quasi-relativistic (QR) method. In QR method, unlike in other perturbation approaches, the relativistic corrections to the valence density due to the first-order relativistic operators are calculated variationally up to all orders. Consequently, the total Kohn-Sham electronic energy can be written as a functional of the quasi-relativistically modified density[39]:

$$E^{QR}[\rho^{QR}] = E^{NR}[\rho^{QR}] + \sum_{i}^{n_{val}} \int d\vec{r}_1 \Psi_i^{QR*} h^{QR} \Psi_i^{QR} \qquad (3.1)$$

where the sum in the second term runs over occupied valence electrons and the constant core terms are omitted from both of the terms here. Given in atomic units, the first-order relativistic operator

$$h^{QR} = h^{MV} + h^{Dar} + h^{SO} \tag{3.2}$$

contains the mass-velocity operator

$$h^{MV} = -\frac{1}{8c^2}\vec{p}^4, \tag{3.3}$$

the Darwin operator

$$h^{Dar} = \frac{1}{8c^2}\Delta(V_N + V_{el}), \tag{3.4}$$

and the spin-orbit (SO) operator

$$h^{SO} = \frac{1}{4c^2}\vec{\sigma}\cdot\left[\vec{\nabla}(V_N + V_{el})\times\vec{p}\right], \tag{3.5}$$

where V_N and V_{el} refers to the nuclear and electron potential, respectively. $\vec{\sigma}$ is the electron spin operator. h^{QR} is the one-electron form of Pauli Hamiltonian. However, combined with the frozen-core approximation, the QR method elegantly bypasses the unboundness problem inherent in the Pauli Hamiltonian. In Eq.(3.1), $E^{NR}[\rho^{QR}]$ is the nonrelativistic energy expressed in terms of the quasi-relativistic Kohn-Sham orbitals that are obtained as the solution to the quasi-relativistic Kohn-Sham equation:

$$f^{QR}\Psi_i^{QR}(\vec{r}_1) = \varepsilon_i^{QR}\Psi_i^{QR}(\vec{r}_1), \tag{3.6}$$

by requiring that $E^{QR}[\rho^{QR}]$ is minimized with respect to the quasi-relativistic valence density ρ_V^{QR} given as

$$\rho_V^{QR}(\vec{r}_1) = \sum_i^{n_{Val}} \Psi_i^{QR*}(\vec{r}_1)\Psi_i^{QR}(\vec{r}_1) \tag{3.7}$$

The QR Kohn-Sham operator can be written as

$$f^{QR}(\vec{r}_1) = h^{NR}(\vec{r}_1) + h^{QR}(\vec{r}_1) \tag{3.8}$$

with $h^{NR}(\vec{r}_1)$ representing the nonrelativistic Kohn-Sham operator[25]. For closed-shell systems, spin-orbit effects can often be neglected and $h^{QR}(\vec{r}_1)$ is replaced by the scalar relativistic (SR) operator $h^{SR}(\vec{r}_1)$ that includes only the MV and Darwin terms. The related SR Kohn-Sham operator serves as a basis of our relativistic modification schemes.

B. Formulation of the scalar relativistic correction schemes

In nonrelativistic theory, the four operators (FC, PSO, DSO, and SD) that give rise to the nuclear spin-spin coupling can be derived from the nonrelativistic Hamiltonian by applying the minimal coupling ($\vec{p} \rightarrow \vec{p} + e\vec{A}$) to the momentum operator and including an extra term that accounts for the interaction between the electron spin and the magnetic field due to nuclei ($\vec{\sigma} \cdot \vec{B}$). These operators are widely known as hyperfine terms, since they describe the interaction between electrons and nuclei. These interactions then give rise to the indirect nuclear spin-spin coupling via the so-called double perturbation. Rigorously, the relativistic spin-spin coupling constant should be calculated from the relativistic hyperfine terms, which can be derived from the Dirac Hamiltonian or some approximate two-component Hamiltonian such as ZORA[90]. Because relativistic hyperfine terms require at least a two-component wavefunction, calculation of the spin-spin coupling is often very time consuming. The goal of this work is however to devise some approximate schemes that can account for most of the relativistic effects on the nuclear coupling while still maintaining the computational ease of the non-relativisitc approach. As stated in the previous section, the mass-velocity correction and Darwin term introduce the major scalar relativistic modifications to the electronic structure. This would in turn influence the nuclear spin-spin couplings even if the hyperfine interactions stay formally unaltered. On the basis of these considerations, our first approach (we shall call it SRI) to estimate relativistic effects on the coupling constant involves the scalar QR Hamiltonian and utilizes the nonrelativistic hyperfine operators. Here, the scalar relativistic reduced spin-spin coupling tensor is expressed as the second derivative of the scalar QR energy:

$$K(A,B)_{ij}^{SRI} = \left.\frac{\partial^2 E^{SR}}{\partial \mu_A^i \partial \mu_B^j}\right|_{\mu_A^i=\mu_B^j=0} \quad \text{with } i,j \in \{x,y,z\}, \tag{3.9}$$

In the above equation, E^{SR} is the total scalar relativistic electronic energy, i and j run over the three cartesian components, and μ_A^i, μ_B^j represent the magnetic moments due to nucleus A and B respectively. The evaluation of $K(A,B)_{ij}^{SRI}$ follows the same procedures[78] as for the nonrelativistic coupling tensor, except that now the unperturbed

orbitals are derived from the QR Hamiltonian. Also, the FC perturbation is now added to the QR KS operator to yield the perturbed spin density matrix. Thus, the isotropic DSO and PSO contributions can be written in SI units as:

$$K(A,B)_{ii}^{SRI,DSO} = \frac{\mu_0{}^2 e^2}{16\pi^2 m_e}\sum_k^{occ}\int \Psi_k^{QR^*}(\vec{r}_1)\frac{(\vec{r}_A\cdot\vec{r}_B)-r_A^i r_B^i}{r_A{}^3 r_B{}^3}\Psi_k^{QR}(\vec{r}_1)\mathrm{d}\vec{r}_1 \tag{3.10}$$

and

$$K(A,B)_{ii}^{SRI,PSO} = -2\left(\frac{\mu_0\beta}{2\pi}\right)^2\sum_k^{occ}\sum_l^{vir}\frac{\int\Psi_k^{QR^*}(\vec{r}_1)h^{(\mu'_{A,PSO})}\Psi_l^{QR}(\vec{r}_1)d\vec{r}_1}{\varepsilon_k^{QR}-\varepsilon_l^{QR}}$$
$$\int\Psi_l^{QR^*}(\vec{r}_1)h^{(\mu'_{B,PSO})}\Psi_k^{QR}(\vec{r}_1)d\vec{r}_1 \tag{3.11}$$

where

$$h^{(\mu'_A,PSO)} = \frac{1}{r_A{}^3}(\vec{r}_A\times\vec{\nabla}) \text{ and } h^{(\mu'_B,PSO)} = \frac{1}{r_B{}^3}(\vec{r}_B\times\vec{\nabla})_i. \tag{3.12}$$

In the above equations, Ψ_k^{QR} denotes the unperturbed QR KS orbitals obtained via Eq. (3.6), β and μ_0 represent the Bohr magneton and vacuum permeability respectively. The final formula for the FC contribution is given by:

$$K(A,B)_{ii}^{SRI,FC} = \frac{2\mu_0\beta}{3}\sum_r^{AO's}\sum_s^{AO's}P_{rs}^{QR,(\mu'_A,FC)}\phi_r^{QR}(\vec{r}=\vec{r}_B)\phi_r^{QR}(\vec{r}=\vec{r}_B), \tag{3.13}$$

with $P_{rs}^{QR,(\mu'_A,FC)}$ being the first-order spin-density matrix in basis of QR atomic orbitals $\phi_r^{QR}(\vec{r})$ and is determined via:

$$P_{rs}^{QR,(\mu'_A,FC)} = \frac{P_{rs}^{QR,\alpha}(\lambda)-P_{rs}^{QR,\beta}(\lambda)}{\lambda}, \tag{3.14}$$

where $P_{rs}^{\alpha}(\lambda), P_{rs}^{\beta}(\lambda)$ are the perturbed density matrix for α and β spin, respectively. These density matrices are constructed from the perturbed KS orbitals obtained by solving the KS equations with a finite Fermi-contact perturbation self-consistently:

$$\left\{f^{QR}[\rho^{QR}]+\lambda\delta(r_A)\sigma_z\right\}\Psi_k^{FC} = \varepsilon_k^{FC}\Psi_k^{FC}. \tag{3.15}$$

Here, λ is the finite perturbation parameter, $f^{QR}[\rho^{QR}]$ is the scalar KS operator as a functional of the unperturbed QR density, and $\delta(r_A)$ is the Dirac Delta function. The

superscript FC is used for KS orbital functions and energies to emphasize that they are perturbed by the Fermi-contact term.

Relativity has impact on each of the three contributions to the nuclear coupling. However, the relativistic correction to the FC contribution is presumably the largest for two reasons. First, the FC term is the predominant contributor to the total coupling. Second, since the FC operator describes the electron-nuclear interaction at the nuclear site, the FC contribution is most sensitive to relativistic effects. According to Eq. (3.13), the FC contribution suffers the relativistic orbital contraction, which affects both the first-order spin-density matrix $P_{rs}^{(\mu_A^1,FC)}$ and the atomic orbital values: $\phi_r(\vec{r}=\vec{r}_B)$ and $\phi_s(\vec{r}=\vec{r}_B)$. However, since we are dealing with couplings involving only one heavy atom, we can deliberately choose the light atom as the perturbing center A and neglect the relativistic effects on the first-order density matrix due to the perturbation of the light atom. In other words, we need to take into account only the relativistic effects on $\phi_r(\vec{r}=\vec{r}_B)$ and $\phi_s(\vec{r}=\vec{r}_B)$. Our previous experience has shown that choosing the lighter atom as the perturbing center gave rise to results that are numerically stable with respect to computational parameters.[78] Based on these considerations, we can write down an approximate form for the relativistically corrected FC contribution as:

$$K(A,B)_{ii}^{SRII.FC} = \frac{2\mu_0\beta}{3}\sum_{r}^{AO's}\sum_{s}^{AO's} P_{rs}^{NR.(\mu_A^1.FC)}\phi_r^{QR}(\vec{r}=\vec{r}_B)\phi_r^{QR}(\vec{r}=\vec{r}_B), \qquad (3.16)$$

where $\phi_r^{QR}(\vec{r}=r_B)$ is obtained from the QR calculation for atomic B, and $P_{rs}^{NR.(\mu_A^1.FC)}$ corresponds to the nonrelativistic form of Eq.(3.14). In contrast to the SRI approach, SRII scheme is computationally less expensive, because only QR atomic calculation is required in addition to computing the nonrelativistic spin-spin coupling.

3.2.3 Computational details

All calculations were performed using the NMR spin-spin coupling code[2,6], which was implemented within the Amsterdam Density Functional (ADF) package[4,5]. The SRII correction was carried out with an auxiliary program. We chose all-electron triple zeta plus double polarization (ADF set V) basis for the coupling ligand atoms, while for the metal and other ligand atoms the frozen-core triple zeta plus single polarization (ADF set IV) basis sets were employed. The valence space for the coupling transition and main-group metals contains subvalence in addition to the true valence electrons. In the self-consistent finite perturbation procedure of calculating FC contribution, the ligand atoms were always used as perturbing center[78] and the perturbation parameter was set to 10^{-3}.

In the calculation of coupling constants involving main-group elements, the experimental structure parameters from the following references are used: Ref 91 for CH_4; Ref 92 for SiH_4, GeH_4; and SnH_4; Ref 93 for $Zn(CH_3)_2$, and $Cd(CH_3)_2$; Ref 94 for $Hg(CH_3)_2$; Ref 95 for $[Zn(CN)_4]^{2-}$; Ref 96 for $[Cd(CN)_4]^{2-}$; Ref 97 for $[Hg(CN)_4]^{2-}$. For PbH_4 the theoretically optimized bond length from Ref 98 is adopted.

In the calculation of couplings involving platinum atom, the structure data for $[Pt(NH_3)_4]^{2+}$ and $Pt(PF_3)_4$ are taken from Ref 99 and Ref 100, respectively. The metal-ligand bond distances as well as angles between them for *cis*-, *trans*-$PtCl_2(PMe_3)_2$, and *cis*-, *trans*-$PtCl_4(PEt_3)_2$ are taken from Ref 101, while the metric data for the ligands are taken from compilations of crystal structure data.[102] For *cis*- and *trans*-$PtCl_2(NH_3)_2$, we assume R(Pt-N)=2.05Å, R(Pt-Cl)=2.50Å, θ(NPtN)=90°, (N-H)=1.01Å, and θ(NPtN)=109.5° based on the crystal structure data[103,102] and theoretical calculation[104]. The structure data for *cis*- and *trans*-$PtH_2(PMe_3)_2$ are taken from ref[105], where Pt-H bond distance for the *cis* isomer is computationally optimized.

3.3 Results and Discussions

3.3.1 Couplings to main-group metals

In order to test the scalar relativistic correction schemes described in the last section, we calculated the one-bond coupling constants for a series of group 4 and 12 compounds. Table 3.1 presents the total coupling constants obtained with the nonrelativistic method (K^{NR}), the quasi-relativistic scalar correction SRI (K^{SRI}) and SRII (K^{SRII}) in comparison with experimental values (K^{Exp}). Overall, the SRII scheme gives better results than the SRI method. It can also be seen that relativity already starts to take effect on couplings involving the fourth-row elements such as Zn and Ge. An increase of 15% seems to be an average for couplings to H or C. For the sixth-row elements Pb and Hg, the SRII scheme enhances the total coupling constants by 70%, 96% and 70% for PbH_4, $Hg(CH_3)_4$, and $[Hg(CN)_4]^{2-}$, respectively. With the experimental values as reference, a factor of 2 seems to be appropriate as a rough estimate of the relativistic increase. If this were true, then we could ascribe the large discrepancy between the predicted and measured coupling constant in $Pb(CH_3)_4$ to the underestimation before relativistic effects are taken into account. According to the nonrelativistic calculation, a relativistic increase factor of 550% would be anticipated to recover the experimental value, which seems to be unreasonable.

Table 3.1. Calculated one-bond reduced coupling constants (in 10^{19} J^{-1} T^{2}) for some main-group 4 and 12 compounds using nonrelativistic method and SRI and SRII schemes.

Molecule	Coupling	K^{Exp}	K^{NR}	K^{SRI}	K^{SRII}
SiH_4	K(Si-H)	84.79[a]	88	87	89
GeH_4	K(Ge-H)	232[b]	188	207	217
SnH_4	K(Sn-H)	431[a]	294	304	293
PbH_4	K(Pb-H)	923[c]	501	629	851
$Ge(CH_3)_4$	K(Ge-C)	-	86	89	108
$Sn(CH_3)_4$	K(Sn-C)	302[d]	195	187	201
$Pb(CH_3)_4$	K(Pb-C)	396[d]	72	-147	207
$Zn(CH_3)_2$	K(Zn-C)	-	299	309	349
$Cd(CH_3)_2$	K(Cd-C)	797[e]	485	488	634
$Hg(CH_3)_2$	K(Hg-C)	126[e]	666	460	1309
$[Zn(CN)_4]^{2-}$	K(Zn, C)	465[e]	405	449	458
$[Cd(CN)_4]^{2-}$	K(Cd, C)	855[e]	648	794	821
$[Hg(CN)_4]^{2-}$	K(Hg, C)	2832[e]	1039	1471	1857

[a]From Reference 59. [b]Form Reference 60.

[c]Taken from the measured coupling constant ^{1}J(Pb-H) in $PbH(CH_3)_3$.[61]

[d]From Reference 62. [e]From Reference 63.

Because of their simplicity, group 4 tetrahydrides are perhaps the best model compounds for investigation of relativistic effects due to a heavy metal on the spin-spin coupling. For the purpose of assessing the quality of the DFT based calculations and studying the effects of electron correlation, we carried out calculations with several different XC functionals. These include LDA[35] and GGA type of functionals due to Becke and Perdew (BP86)[122-123], Perdew and Wang (PW91)[106] and Becke, Lee, Yang and Parr (BLYP)[122,124]. It is found that LDA gives results roughly 10% smaller than BP86, while other GGA functionals yield values very close to BP86. Therefore, we shall

focus on comparison of the BP86 and LDA results. In Table 3.2, all contributions obtained with BP86 and LDA without relativistic corrections are presented. We also show the few available numbers from the MCSCF calculations[88]. Comparing LDA with BP86, we note that all FC and PSO contributions from the BP86 calculations are larger in magnitude. The DSO contributions are numerically very small and will therefore not be discussed. The change in the FC contribution induced by the gradient correction (also called nonlocal correction) to the density functional can be attributed to the change in electron density due to the gradient correction. Fan and Ziegler[126] have shown that nonlocal corrections generally increase the density at the core region and the valence tail. Since the FC contribution is extremely sensitive to the change in the core region of the valence orbitals, the increase due to nonlocal corrections is readily understandable. The fact that the BP86 results compare better with experimental values is another proof that nonlocal corrections are important for describing sensitive molecular properties such as nuclear couplings. Comparing DFT results with Hartree-Fock (HF) and post-HF results, we find that for the PSO and DSO contributions, which are singlet properties, DFT agrees extremely well with the HF-based methods. For FC contributions, a triplet property, DFT generally gives lower values than RPA and MCSCF based approaches. The only exception is SiH_4, where BP86 yields higher coupling constant than CAS B does. It is interesting to note that the nonrelativistic MCSCF calculations agree perfectly with experiments for GeH_4 and SnH_4 and as a consequence leave no room for any relativistic corrections in contrast to DFT calculations. However, as mentioned before, it seems peculiar that our scalar relativistic scheme does not give any correction to the coupling ^1K(Sn-H). Also, even with relativistic correction, DFT based ^1K(Ge-H) is smaller than the measured value. All these facts indicate that there is an underestimation on the nonrelativistic level for the DFT approach. However, since, as seen from Table 2, the spin-orbit effects are of no importance for all couplings, and there are no scalar relativistic *ab initio* results available, it remains unclear to which extent the DFT results are underestimated.

Table 3.2 Comparison of DFT, HF and post-HF calculations[a] for one-bond coupling constants in group 4 tetrahydrides.

Complex	Method	K_{FC}^{NR}	K_{PSO}^{NR}	K_{DSO}^{NR}	K_{Tot}^{NR}	$K_{Corr}^{Rel\ b}$	K^{Exp}
SiH_4	BP86	88.3	-0.170	0.013	88.1	0.5	84.79
	LDA	75.9	-0.144	0.014	75.7	1.2	
	RPA	96.64	-0.138	0.0084	96.51	0.025	
	CAS B	78.21	-0.084	0.0126	78.14		
GeH_4	BP86	189.0	-0.482	0.019	188.5	28.2	232
	LDA	170.0	-0.362	0.016	169.65	25.6	
	RPA	300.74	-0.547	0.0238	300.22	0.169	
	CAS B	232.66	-0.499	0.0238	232.18		
SnH_4	BP86	295.5	-1.221	0.013	294.3	-1.3	431
	LDA	266.7	-1.074	0.013	265.6	0.6	
	RPA	485.48	-1.394	0.0067	484.09	4.71	
	RAS B	421.75	-1.227	0.0067	420.53		
PbH_4	BP86	504.3	-2.81	0.010	501.5	349.2	923
	LDA	442.1	-2.54	0.010	439.6	312.3	

[a]Results taken from Reference 88. RPA refers to the lower level random-phase approximation (RPA) while CAS B and RAS B refer to the correlated results with CAS B and RAS B as reference MCSCF wavefunctions.

[b]Scalar relativistic corrections with SRII scheme are listed for BP86 and LDA calculations. The spin-orbit corrections are shown for RPA results.

Finally, we shall give some comments on the relativistic effects on the spin-spin coupling and try to understand why the SRII correction scheme works better. As already known, effects of relativity manifest themselves in both the molecular geometry and electronic structure.[107] The former can be observed in the contraction of the bond length when one (or both) of the bonding atoms belongs to the fifth- or higher row elements in the periodic table. The latter gives rise to the orbital contraction and stabilization (s and

p) as well as the orbital expansion and destabilization (d and f). It seems surprising that although the relativistic effects on KS orbitals are fully taken into account in our SRI scheme, it gives less improvement than the SRII scheme where only the s-contraction is accounted for. This may be attributed to the deficiency in the current implementation of the quasi-relativistic approach, where the valence orbitals are subjected to the relativistic core potential but orthogonalized onto the nonrelativistic core orbitals. Also, it is difficult to justify whether the simple incorporation of the nonrelativistic hyperfine terms to the Pauli Hamiltonian is an appropriate approach to satisfactorily treat the relativistic effects on the spin-spin coupling. On the other hand, the consequences of the approximate SRII approach are more apparent, since it only accounts for the s-orbital contraction, which is the predominant relativistic effect on the contact-type nuclear spin-spin interactions.

3.3.2 Couplings to Platinum

To examine the validity of the proposed relativistic correction scheme SRII for couplings involving transition metals, we have performed calculations on some platinum complexes. Table 3.3 presents both predicted and experimental ^{1}K(Pt-N) and ^{1}K(Pt-P) for some platinum amine and platinum phosphine complexes. Again, it can be seen that SRII correction is able to recover most of the anticipated relativistic increase with an average deviation of around 25% from experiment, whereas the SRI method fails completely.

Table 3.3 Calculated one-bond reduced coupling constants (in 10^{19} J^{-1} T^2) for some platinum using nonrelativistic method and scalar relativistic correction SRI and SRII schemes.

Molecule	Coupling	K^{Exp}	K^{NR}	K^{SRI}	K^{SRII}
$[Pt(NH_3)_4]^{2+}$	K(Pt-N)	1089[a]	605	599	999
c-$PtCl_2(NH_3)_2$	K(Pt-N)	1154[b]	411	150	730
t-$PtCl_2(NH_3)_2$	K(Pt-N)	1059[b]	496	368	891
$Pt(PF_3)_4$	K(Pt-P)	6215[c]	2981	3770	5433
c-$PtCl_2(PMe_3)_2$	K(Pt-P)	3316[d]	1487	1609	2286
t-$PtCl_2(PMe_3)_2$	K(Pt-P)	2267[d]	867	892	1433
c-$PtH_2(PMe_3)_2$	K(Pt-P)	1786[d]	893	654	1474
t-$PtH_2(PMe_3)_2$	K(Pt-P)	2472[d]	1200	839	1832
c-$PtCl_4(PEt_3)_2$	K(Pt-P)	1976[e]	946	978	1602
t-$PtCl_4(PEt_3)_2$	K(Pt-P)	1386[e]	695	626	1131

[a]From Reference 119. [b]From Reference 120. [c]From Reference 68. [d]From Reference 111. [e]From Reference 110.

By comparing K^{SRII}/K^{NR} with K^{Exp}/K^{NR}, Figure 3.1 shows how the calculated relativistic correction is related to the experimentally predicted relativistic increase. From the shape of the curve K^{EXP}/K^{NR} it is obvious that the extent of relativistic modification depends on the chemical environment of the coupling nucleus. This can certainly not be described by the "hydrogen-like" relativistic correction of Pyykkö[83], where a multiplicative factor is assigned for each heavy metal and applied on top of the nonrelativistically calculated total coupling constants. In contrast, our SRII correction can mimic the trend of relativistic influence in different ligand environments to a certain degree. Evidently, our correction is more flexible than the "hydrogen-like" correction.

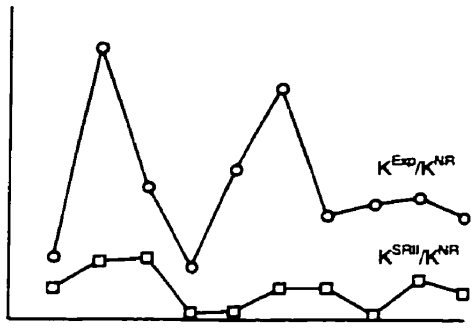

Figure 3.1 Correlation between the calculated and experimentally predicted relativistic increase in coupling constants for some platinum complexes.

The thermodynamic *trans* influence, defined as the extent to which a ligand labilizes the bond opposite to itself in the ground state, is a well-established concept in transition-metal chemistry.[108,109] The *trans* influence is experimentally measurable through the use of X-ray crystallography, vibrational spectroscopy, nuclear magnetic resonance, nuclear quadrupole resonance, and photoelectron spectroscopy. The order of *trans* influence obtained by these techniques for common ligands is similar but not unique since it reflects one or more aspects of the electronic structure of the complex. Maybe the most widely known *trans* influence series is provided by the determination of the bond length M-A that is *trans* to the influencing ligand L. Consequently, ligands such as amine, chloride, phosphine and hydride in square planar Pt(II) complexes can be placed in the order of their structural *trans* influence as:[108] $NH_3 \approx Cl^- < PR_3 < H^-$. In our discussion, we will refer the influencing ligand L to the ligand which exerts a stronger *trans* influence according to this series.

The connection between *trans* influence and the magnitude of NMR coupling constants for stereoisomers of platinum square planar and octahedral systems was discussed in Ref. 108, 110 and 111. Thus, for the complexes $PtCl_2(PR_3)_2$, a greater value of ^1K(Pt-P) is always observed for the *cis* isomers than for the *trans* isomers. It was proposed that the *trans* influence of a ligand is to reduce the s-character of the platinum

hybrid orbital and consequently to decrease the coupling between platinum and phosphorus. [112,113] However, until now no first-principles calculation has addressed this issue. Therefore, it seems worthwhile to investigate this relation through DFT based calculations. The first important question in this conjunction is whether the difference in the coupling constant for *cis* and *trans* isomers can be ascribed to the difference in the bond distance due to the structural *trans* influence as addressed in Ref. 110. For this purpose, we shall examine how the calculated ^1K(Pt-P) changes at various bond lengths, angles and geometrical arrangements.

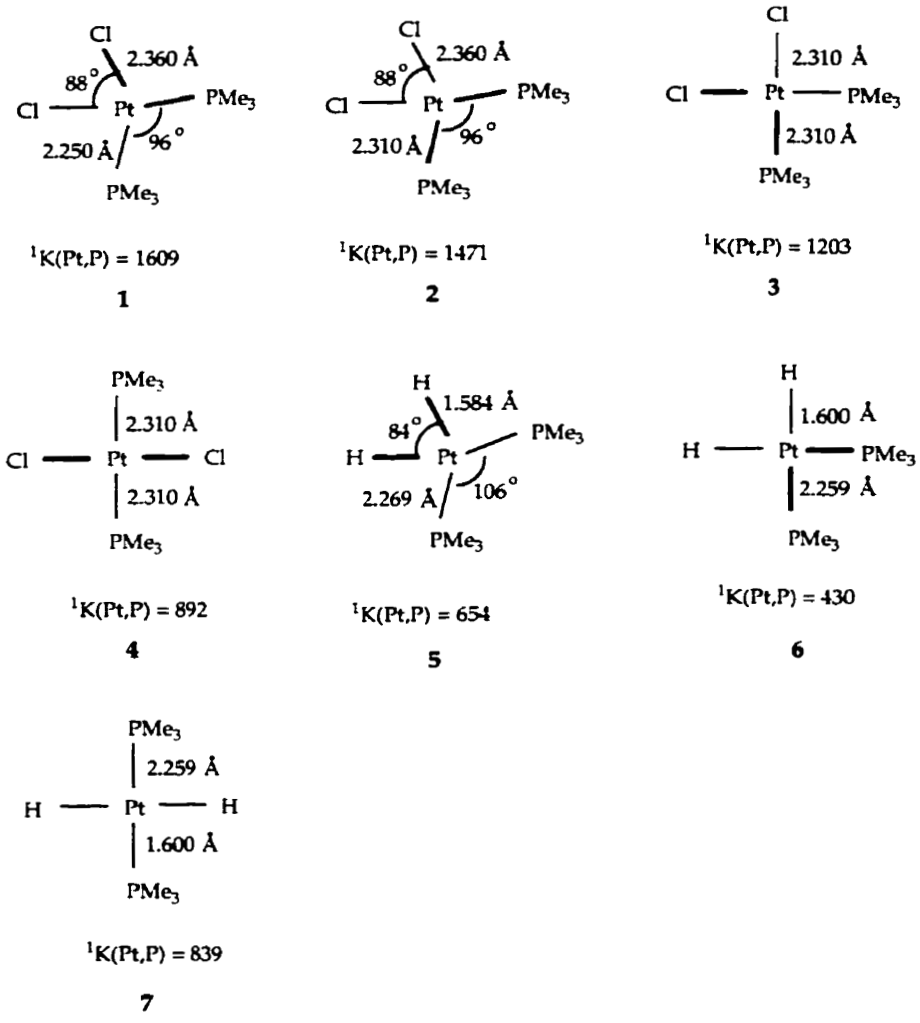

Figure 3.2 The dependence of the coupling constants (calculated with SRI correction scheme) on the structural parameters.

It can be seen from Figure 3.2 that, if R(Pt-P) is increased from 2.25 Å in the equilibrium geometry of *cis*-$Cl_2(PMe_3)_2$, **1**, to 2.31 Å, **2**, ^1K(Pt-P) decreases from 1609 to 1471 (10^{19} J^{-1} T^2). At this new bond distance R(Pt-P), if R(Pt-Cl) is shortened to 2.31 Å, and the angles θ(P-Pt-P), θ(Cl-Pt-Cl) are arranged to be 90°, **3**, ^1K(Pt-P) reduces further to 1203 (10^{19} J^{-1} T^2), which is about 25% lower than the value at the equilibrium geometry, **1**. Finally, keeping the bond lengths and angles fixed, if the position of one chlorine ligand is exchanged with that of one phosphine ligand, **4** (the equilibrium geometry of *trans*-$PtCl_2(PMe_3)_2$), ^1K(Pt-P) goes further down by about 20% to 892 (10^{19} J^{-1} T^2). Similar calculations have also been conducted for $PtH_2(PMe_3)_2$ isomers. They reveal a variation of ^1K(Pt-P) from 654 at the *cis* geometry, **5**, over 430, at the bond distance and angles from the *trans* configuration, **6**, to 839 (10^{19} J^{-1} T^2), at the *trans*-geometry, **7**. Thus, apart from the outcome of the structural *trans* influence, there is a more important electronic factor that determines the spin-spin coupling in these square planar systems. This factor explains the change in the coupling in going from the *cis* isomer **3** to the *trans* isomer **4**, or from **6** to **7**. We shall in the following borrow the idea from Burdett and Albright[125] to rationalize this electronic influence.

For an ideal *trans* complex with symmetry D_{2h}, the σ interactions between metal and ligands give rise to three ligand-based occupied MO's: $1a_g$, $2a_g$ and b_{3u}, and the corresponding metal-based anti-bonding virtual orbitals, Figure 3.3. Here, it is assumed that the *trans* influencing ligand is L_2, identical to L_4, and the influenced ligand is L_1, identical to L_3. Obviously, $2a_g$ is the orbital that contributes to the spin-spin coupling.[78] Now if the ligand L_2 is replaced with L_2', which has a higher electronegativity or a lower σ-donor ability, the symmetry of the system is reduced to C_{2v}, with L_2'-M-L_4 as the C_2 axis. Consequently, the initial b_{3u} orbital becomes a total symmetrical orbital $3a_1$, and can be perturbed by the virtual orbital $2a_1^*$ to form a new orbital, which represents the bonding interaction of the metal hybrid sp_x orbital with the σ ligand orbitals *trans* to each other (L_2' and L_4), as shown in Figure 3.4.

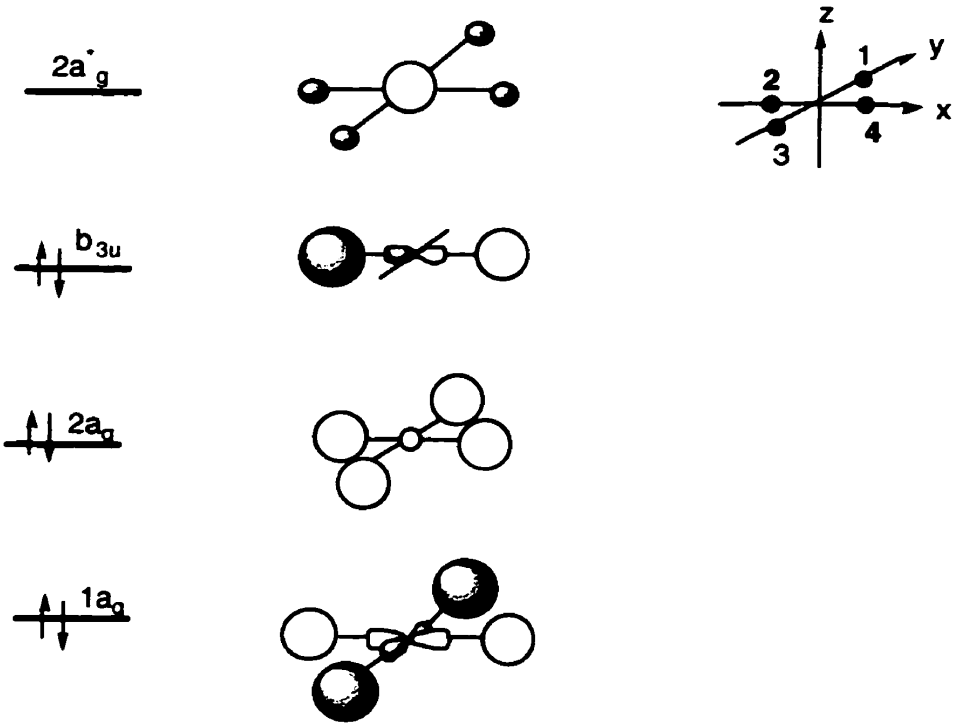

Figure 3.3 The important σ interactions in a *trans* planar complex with symmetry D_{2h}.

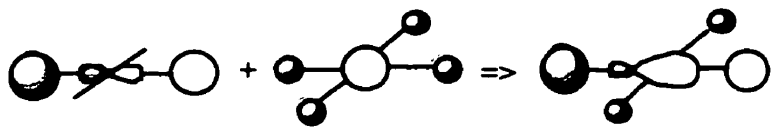

Figure 3.4 The polarization of the virtual orbital on the *trans* σ bond L'-M-L" in a *trans*-$ML_2L'L''$ complex with symmetry C_{2v}.

This perturbation is favored because of the small energy gap between the high-lying occupied orbital $3a_1$ and the low-lying virtual orbital $2a_1$*. Since L_2 has a higher electronegativity, the phase of the mixing is determined such that the resultant orbital has a larger electron density at L_2. It is clear from the shape of this orbital that there is a large overlap population between the metal s-orbital and the σ-orbital at L_4, and hence it can add to the FC term of the M-L_4 spin-spin coupling. In other words, ^1K(M-L_4) becomes larger if the *trans* ligand L_2 is replaced by a weaker σ-donor ligand L_2'. This predicts that

^1K(M-L_4) in *trans*-$PtCl_2(PMe_3)Cl$ should be larger relative to that in *trans*-Pt $Cl_2(PMe_3)_2$, as Cl^- is a weaker σ-donor.

Let us examine now the situation when the position of L_2 is switched with that of L_1. In this case, the molecule still transforms as C_{2v}, but with the C_2 axis cutting through the two identical ligands. Consequently, the initial $2a_g^*$ orbital will mix with an occupied orbital that is a linear combination of the initial orbitals b_{2u} and b_{3u}, and gives rise to a new bonding orbital that contains a large overlap population between the metal s-orbital and both of the σ-orbitals from L_4 and L_2, Figure 3.5. Therefore, the coupling ^1K(M-L_4) is anticipated to increase with respect to the original *trans* configuration. This explains why ^1K(M-P) for *cis*-$PtCl_2(PMe_3)_2$ is larger than that for its *trans* isomer.

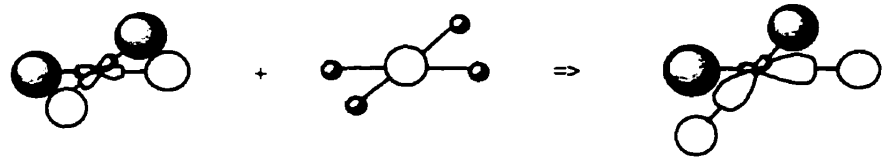

Figure 3.5 The polarization of the virtual orbital on the *trans* σ bond L-M-L′ in a *cis*-$ML_2L'_2$ complex with symmetry C_{2v}.

After establishing the link between electronic *trans* influence, σ-donor ability and the magnitude of spin-spin coupling constants, we can understand the results for other stereoisomers of Pt(II) and Pt(IV) complexes. Our calculations show a slightly larger coupling for *trans*- than for *cis*-$PtCl_2(NH_3)_2$, Table 3.3. However, experimental values give a reversed trend. This can be explained, as the σ-donor abilities of Cl^- and NH_3 are very close and our approximate method may not be able to pick up the fine difference. For hydrido phosphine complexes, both theoretically and experimentally the *trans*-isomer exhibits larger ^1K(Pt-P) since the hydrido ligand is a stronger σ-donor than phosphine. Moving to the octahedral Pt(IV) complexes $PtCl_4(PEt_3)_2$, it is noted that Pt-P coupling is much smaller than the analogous square planar complexes. The correlation of the oxidation state with the magnitude of the coupling constant is however accidental. As pointed out in Ref. 78, complexes with a larger coordination number generally should

have smaller coupling constants, owing to the smaller normalization factor $1/\sqrt{n}$, where n represents the coordination number.

3.4 Concluding remarks

Based on the nonrelativistic hyperfine operators, two approximate frozen-core scalar relativistic corrections are devised to account for the major relativistic effects on one-bond metal-ligand nuclear spin-spin coupling constants. In the first scheme, SRI, the quasirelativistic approach is incorporated into the nonrelativistic coupling calculation. In the second scheme, SRII, a refined version of Pyykkö's "hydrogen-like" hyperfine correction is used, which only involves the correction of the s orbital value at the heavy nucleus in the evaluation of the Fermi-contact contribution.

The calculations have revealed that SRII gives significant improvement over SRI for couplings to sixth-row main-group elements. It is also able to satisfactorily recover the bulk of the relativistic increase for couplings to platinum and reproduce the experimental trends in different ligand environment due to the relativistic effects, whereas SRI scheme fails almost completely. We rationalize this, as the SRII method accounts for the s-orbital contraction, which is the predominant relativistic effect on the contact-type nuclear spin-spin interactions. However, one of the limitations of this scheme is that it can treat couplings involving only one heavy nucleus. Also, owing to its highly qualitative nature, an approach to the systematic improvement of the correction is not obvious. Therefore, a rigorous approach departing from a relativistic hyperfine operator would be desirable.

Finally, as an interesting application, the connection between the structural *trans* influence and the magnitude of coupling constants has been explored on the basis of the calculations. It has been found that, although the metal-ligand bond distance and angles influence the magnitude of the coupling, the major factor that give rise to the difference between *cis* and *trans* configuration is of electronic nature. This can be attributed to the change in the overlap population between the metal s and ligand σ orbitals under the

influence of a *trans* ligand, which is caused by the polarization of the anti-bonding virtual orbital (between metal s and ligand σ orbitals) on the occupied *trans* σ bonds.

Chapter 4
Summary and Future Prospects

The goal of this thesis was to develop and apply DFT based methodologies to the study of nuclear spin-spin couplings. Towards this goal, an existing nonrelativistic implementation was applied to the study of metal-ligand NMR coupling constants in a series of transition-metal systems. In the course of the calculations, insight into the origin of the Fermi-contact and paramagnetic spin-orbit coupling contribution has been gained by means of a molecular orbital-based analysis. Also, rationales have been found to explain the trends and to qualitatively predict the size of the coupling constants based on some simple criteria. It was also demonstrated that nuclear spin-spin coupling is a valence property, which allows the adoption of frozen-core approximation to facilitate applications to heavy-metal systems. However, in order to study NMR couplings in these systems, a relativistic approach has to be developed to model the relativistic effects. Towards this goal, two approximate frozen-core relativistic correction schemes have been developed and evaluated on one-bond couplings to heavy main-group and transition metal atoms. It was found that a simple correction that accounts only for the relativistic contraction of s orbitals at the heavy metal nucleus can satisfactorily recover the bulk of the relativistic increase in the metal-ligand coupling constants for both main-group and transition-metal systems. The relationship between the *trans* influence and coupling constants was examined on the basis of the calculations and rationalized using a perturbation theory-based molecular orbital approach.

One of the limitations of the presented relativistic correction scheme is that it can treat couplings involving only one heavy nucleus. Also, owing to its highly qualitative nature, an approach to the systematic improvement of the correction is not obvious. Therefore, a rigorous approach departing from a relativistic hyperfine operator would be desirable. One of such methods is based on the ZORA (zeroth-order regular approximation) hamiltonian[90], which can be derived from the Dirac hamiltonian using an

alternative expansion in contrast to the Pauli hamiltonian. ZORA hamiltonian was shown to be able to describe near-nuclear region more accurately than the Pauli hamiltonian. Also, it is variationally stable and has been shown to yield better energies and wavefunctions, especially for the ultra relativistic elements such as Gold and Uranium. Below is a brief derivation of the relativistic hyperfine operators from the ZORA hamiltonian. The details and the description of possible implementation in ADF is given in reference 121.

By replacing the nonrelativistic Pauli kinetic energy operator with the corresponding ZORA kinetic operator, one can obtain the ZORA Kohn-Sham operator:

$$h^{ZORA} = V_{eff} + \vec{\sigma}\cdot\vec{p}\frac{K}{2}\vec{\sigma}\cdot\vec{p} = V_{eff} + \vec{p}\cdot\frac{K}{2}\vec{p} + i\vec{\sigma}\cdot(\vec{p}\times\frac{K}{2}\vec{p}). \tag{4.1}$$

Here V_{eff} is the effective potential which is the sum of the nuclear, coulomb and XC potentials, $\vec{\sigma}$ is the Pauli spin matrices, and $K = \frac{1}{1 - V/2c^2}$.

By introducing the minimal coupling: $\vec{p} \rightarrow \vec{\Pi} = \vec{p} + \frac{\vec{A}}{c}$, the magnetic field-dependent ZORA KS operator, after some manipulations, can be written as,

$$\begin{aligned} h^{ZORA} = V &+ \vec{p}\cdot\frac{K}{2}\vec{p} + \vec{p}\cdot\vec{A}\frac{K}{2c} + \frac{K}{2c}\vec{A}\cdot\vec{p} + \frac{K}{2c^2}A^2 \\ &+ \frac{1}{2}\vec{\sigma}\cdot(\vec{\nabla}K\times\vec{p}) + \frac{1}{2c}\vec{\sigma}\cdot(\vec{\nabla}K\times\vec{A}) + \frac{K}{2c}\vec{\sigma}\cdot\vec{B} \end{aligned} \tag{4.2}$$

The magnetic moment of a nucleus arising from the nuclear spin and the related magnetic vector potential are given by:

$$\vec{\mu}^v = \frac{g_v}{2Mc}\vec{I}^v \text{ and } \vec{A}^v = \frac{\vec{\mu}^v\times\vec{r}_v}{r_v^3}\text{ , respectively,} \tag{4.3}$$

where g_v is the nuclear g value, M is the proton mass, I_v is the nuclear spin and $\vec{r}_v$ is the position vector relative to the nucleus, which defines the gauge. The corresponding magnetic field (flux density) is then:

$$\vec{B}^v = 3\frac{\vec{r}_v(\vec{\mu}_v\cdot\vec{r}_v)}{r_v^5} - \frac{\vec{\mu}_v}{r_v^3} + \frac{8\pi}{3}\delta(r_v)\vec{\mu}_v, \tag{4.4}$$

where a delta function at the nuclear position is introduced. In the presence of two magnetic active nuclei, we have A^1 (or B^1) and A^2 (or B^2) denoting the vector potential (or magnetic field) due to nucleus 1 and nucleus 2, respectively. We are interested in terms within the ZORA operator (Eq. 4.2), which are linear in either the magnetic vector potential or magnetic field due to these nuclei. These terms form the so-called ZORA hyperfine operator:

$$h^{hyperfine} = \frac{g_e}{4c}\{K\vec{\sigma}\cdot(\vec{B}^1+\vec{B}^2)+K(\vec{A}^1+\vec{A}^2)\cdot\vec{p}+\vec{p}\cdot(\vec{A}^1+\vec{A}^2)K \\ +\vec{\sigma}\cdot[\vec{\nabla}K\times(\vec{A}^1+\vec{A}^2)]\}+\frac{g_e^{\,2}}{4c^2}K(\vec{A}^1\cdot\vec{A}^2). \tag{4.5}$$

Here we have introduced a factor of $\left(\frac{g_e}{2}\right)$ to terms linear in the magnetic field to account for the quantum electrodynamics effects. By inserting the explicit form of the magnetic field and vector potential (Eq. 4.3 and 4.4) into Eq. 4.5, the hyperfine operator becomes:

$$h^{hyperfine} = \frac{g_e}{4Mc}\sum_{v=1\text{and }2}\{K\vec{\sigma}\cdot\left(3\frac{\vec{r}_v(\vec{\mu}^v\cdot\vec{r}_v)}{r_v^5}-\frac{\vec{\mu}^v}{r_v^3}\right)+K\frac{8\pi}{3}\delta(\vec{r}_v)\vec{\sigma}\cdot\vec{\mu}^v \\ +K\vec{\sigma}\cdot\left[\vec{\nabla}K\times\left(\frac{\vec{\mu}^v\times\vec{r}_v}{r_v^3}\right)\right]+\frac{1}{r_v^3}(K\vec{\mu}^v\cdot\vec{l}_v+\vec{\mu}^v\cdot\vec{l}_vK)\} \tag{4.6} \\ +\frac{g_e^{\,2}}{4c^2}K\frac{(\vec{\mu}^1\cdot\vec{\mu}^2)(\vec{r}_1\cdot\vec{r}_2)-(\vec{\mu}^1\cdot\vec{r}_2)(\vec{\mu}^2\cdot\vec{r}_1)}{r_1^3r_2^3},$$

where the superscripts (or subscripts) 1 and 2 refer to nucleus 1 and 2, respectively. The first two terms in the hyperfine operator describe the interaction between the electronic and nuclear spin magnetic moments. The first one corresponds to the nonrelativistic spin-dipolar (SD) term and the second one to the Fermi-contact (FC) term. The third term originates from the field-free spin-orbit operator and is called the spin-orbit Zeeman gauge correction (SOZC) term. The last two terms describe the magnetic interaction of the nuclear spin and the electron orbital current and corresponds to the nonrelativistic paramagnetic spin-orbit (PSO) and diamagnetic spin-orbit (DSO) term.

Bibliography

(1) Schreckenbach, G.; Ziegler, T. *J. Phys. Chem.* **1995**, *99*, 606.

(2) Dickson, R. M.; Ziegler, T. *J. Phys. Chem.* **1996**, *100*, 5286.

(3) Parr, R. G.; Yang, W. *Density Functional Theory of Atoms and Molecules*; Oxford University Press: New York, Oxford, 1989.

(4) Baerends, E. J.; Ellis, D. E.; Ros, P. *Chem. Phys.* **1973**, *2*, 41.

(5) Te Velde, G.; Baerends, E. J. *J. Comp. Phys.* **1992**, *99*, 84.

(6) Dickson, R.; Khandogin, J. "The NMR spin-spin coupling code for ADF 2.3," The University of Calgary, July 1999.

(7) Ramsey, N. F. *Phys. Rev.* **1953**, *91*, 303.

(8) Fukui, H. *Magn. Res. Rev.* **1994**, *11*, 205.

(9) Pyykkö, P. *Chem. Rev.* **1988**, *88*, 563.

(10) Pople, J. A.; Santry, D. P. *Mol. Phys.* **1963**, *8*, 1.

(11) Pople, J. A.; McIver, J. W. J.; Ostlund, N. S. *J. Chem. Phys.* **1968**, *49*, 2960.

(12) Pople, J. A.; J.W. McIver, J.; Ostlund, N. S. *J. Chem. Phys.* **1968**, *49*, 2965.

(13) Kowalewski, J.: In *Annual Reports on NMR Spectroscopy*; Webb, G. A., Ed.; Academic Press: London, 1982; Vol. 12.

(14) Geertsen, J.; Oddershede, J.; Scuseria, G. *J. Chem. Phys.* **1987**, *87*, 2138.

(15) Oddershede, J.; Rayners, W. T.; Scuseria, G. E. *J. Phys. Chem.* **1988**, *92*, 3056.

(16) Oddershede, J. *Nucl. Magn. Reson.* **1991**, *20*, 112.

(17) Malkin, V. G.; Malkina, O. L.; Salahub, D. R. *Chem. Phys. Lett.* **1994**, *221*, 91.

(18) Malkina, O. L.; Salahub, D. R.; Malkin, V. G. *J. Chem. Phys.* **1996**, *105*, 8793.

(19) Snijders, J. G.; Baerends, E. J. *Mol. Phys.* **1978**, *36*, 1789.

(20) Snijders, J. G.; Baerends, E. J.; Ros, P. *Mol. Phys.* **1979**, 1909.

(21) Boerrigter, P. M. Ph.D. thesis, Free University, Amsterdam, The Netherlands, 1987.

(22) Ziegler, T.; Tschinke, V.; Baerends, E. J.; Snijders, J. G.; Ravenek, W. *J. Phys. Chem.* **1989**, *93*, 3050.

(23) Hohenberg, P.; Kohn, W. *Phys. Rev.* **1964**, *136*, B864.

(24) Kohn, W.; Sham, L. J. *Phys. rev.* **1965**, *140*, A1133.

(25) Ziegler, T. *Chem. Rev.* **1991**, *91*, 651.

(26) Pyykkö, P.: In *The Effect of Relativity on Atoms, Molecules and Solid State*; Wilson, S., Ed.; Plenum Press: New York, 1991; pp 1.

(27) Moss, R. E. *Advanced Molecular Quantum Mechanics*; Chapman and Hall: London, 1973.

(28) McWeeny, R. *Methods of Molecular Quantum Mechanics*; Academic Press: New York, 1989.

(29) Vignale, G.; Rasolt, M. *Phys. Rev. B* **1988**, *37*, 10685.

(30) Becke, A. D. *Can. J. Chem.* **1996**, *74*, 995.

(31) Baerends, E. J.; Ellis, D. E.; Ros, P. *Chem. Phys.* **1973**, *2*, 41.

(32) Baerends, E. J.; Ros, P. *Chem. Phys.* **1973**, *2*, 51.

(33) Baerends, E. J.; Ros, P. *Int. J. Quant. Chem.: Quant. Chem. Sym.* **1978**, *12*, 169.

(34) Versluis, L.; Ziegler, T. *J. Chem. Phys.* **1988**, *88*, 322.

(35) Vosko, S. H.; Wilk, L.; Nusair, M. *Can. J. Phys.* **1980**, *58*, 1200.

(36) Vernoijis, P.; Snijders, J. G.; Baerends, E. J. *Slater Type Basis Functions for the Whole Periodic System*; Department of Theoretical Chemistry, Free University: Amsterdam: The Netherlands, 1981.

(37) Mann, B. E.; Taylor, B. F. *^{13}C NMR Data for Organometallic Compounds*; Academic Press: , 1981.

(38) Rehder, D.; Bechthold, H.-C.; Kececi, A.; Schmidt, H.; Siewing, M. *Z. Naturforsch.* **1982**, *37b*, 631.

(39) Ziegler, T.; Snijders, J. G.; Baerends, E. J. *Chem. Phys. Lett.* **1980**, *75*, 1.

(40) Ziegler, T.; Snijders, J. G.; Baerends, E. J. *J. Chem. Phys.* **1981**, *74*, 1271.

(41) Ziegler, T.; Snijders, J. G.; Baerends, E. J. "The Challenge of d and f Electrons"; ACS Symposium Series, 1989.

(42) Schwarz, W. H. E.; Wezenbeek, E. M. v.; Baerends, E. M.; Snijders, J. G. *J. Phys. Chem.* **1989**, *B22*, 1515.

(43) Wezenbeek, E. M.; Baerends, E. J.; Ziegler, T. *Inorg. Chem.* **1995**, *34*, 238.

(44) Reibenspies, J. H.; Klausmeyer, K. K.; Darensbourg, D. J. *Z. Kristallogr.* **1995**, *210*, 882.

(45) Lenthe, E. Ph.D. thesis, Free University Amsterdam, Amsterdam, The Netherlands, 1996.

(46) Douglas, M.; Kroll, N. M. *Ann. Phys.* **1974**, *82*, 89.

(47) Barysz, M.; Sadlej, A. J.; Snijders, J. G. *Int. J. Quant. Chem.* **1997**, *65*, 225.

(48) McGlynn, S. P.; Vanquickenborne, L. G.; Kinoshita, M.; Carroll, D. G. *Introduction to Applied Quantum Chemistry*; Holt, Rinehart and Winston, Inc.: , 1972.

(49) Ziegler, T.; Rauk, A.; Baerends, E. J. *Chem. Phys.* **1976**, *16*, 290.

(50) Kaup, M.; Malkina, O. L.; Malkin, V. G. *J. Chem. Phy.* **1997**, *106*, 9201.

(51) Schreckenbach, G.; Ziegler, T. *Int. J. Quant. Chem.* **1997**, *61*, 899.

(52) Beagley, B.; Schmiding, D. G. *J. Mol. Struct.* **1974**, *22*, 466.

(53) Lucken, E. A. C.; Noack, K.; Williams, D. F. *J. Chem. Soc. A* **1967**, *148*.

(54) Calderazzo, F.; englert, U.; Pampaloni, G.; Pelizzi, G.; Zamboni, R. *Inorg. Chem.* **1983**, *22*, 1865.

(55) Jost, A.; Rees, B. *Acta Crystallogr.* **1975**, *B31*, 2649.

(56) Kato, K.; Takayama-Muromachi, E. *Acta Cryst.* **1987**, *C43*, 2040.

(57) MacGinnety, J. A. *Acta Cryst.* **1972**, *B28*, 2845.

(58) Palenik, P. *Inorg. Chem.* **1967**, *6*, 503.

(59) Thiele, A.; Fuchs, J. *Z. Naturforsch.* **1978**, *34b*, 148.

(60) German, K. E.; Grigoryev, M. S.; A.F.Kuzina; Gulev, B. F.; Spitsin, V. I. *Dokl. Akad. Nauk SSSR* **1986**, *287*, 650.

(61) Buckingham, M. J.; Hawkes, G. E. *Inorg. Chim. Acta* **1981**, *56*, L41.

(62) Bode, H.; Voss, E. *Z. Anorg. Allg. Chemie* **1957**, *290*, 1.

(63) Calov, U.; Schneider, M.; Leibnitz, P. *Z. Anorg. All. Chem.* **1991**, *604*, 77.

(64) Halasyamani, P.; Heier, K. R.; Willis, M. J.; Stern, C. L.; Poeppelmeier, K. R. *Z. Anorg. Allg. Chem.* **1996**, *622*, 479.

(65) Hao, N.; Sayer, B. G.; Dénès, G.; Bickley, D. G.; Detellier, C.; McGlinchey, M. J. *J. Magn. Reson.* **1983**, *50*, 50.

(66) Banck, J.; Schwenk, A. *Z. Physik* **1975**, *B 20*, 75.

(67) Marriott, J. C. *Chem. Comm.* **1970**, 595.

(68) Hao, N.; McGlinchey, M. J.; Sayer, B. G.; Schrobilgen, G. J. *J. Mag. Res.* **1982**, *46*, 158.

(69) Dove, M. F. A.; Jones, E. M. L.; Clark, R. J. *Mag. Res. Chem.* **1989**, *27*, 973.

(70) Bailey, J. T.; Clark, R. J.; Levy, G. C. *Inorg. Chem.* **1982**, *21*, 2086.

(71) Helgaker, T.; Jaszunski, M.; Ruud, K. *Chem. Rev.* **1999**, *99*, 293.

(72) Jameson, C. J.; Dios, A. C. d.: In *A Specialist Periodical Report, Nuclear Magnetic Resonance*; Webb, G. A., Ed.; Royal Society of Chemistry, 1999; Vol. 28; Chap. 2.

(73) Oddershede, J.; Geertsen, J.; Scuseria, G. E. *J. Phys. Chem.* **1988**, *92*, 3056.

(74) Perera, S. A.; Sekino, H.; Bartlett, R. J. *J. Chem. Phys.* **1994**, *101*, 2186.

(75) Vahtras, O.; Agren, H.; Jorgensen, P.; Jensen, H. J. A.; Padkjaer, S. B.; Helgaker, T. *J. Chem. Phys.* **1992**, *96*, 6120.

(76) Fukui, H.; Miura, K.; Matsuda, H.; Baba, T. *J. Chem. Phys.* **1992**, *97*, 2299.

(77) Malkin, V. G.; Malkina, O. L.; Salahub, D. R. *Chem. Phys. Lett.* **1994**, *221*, 91.

(78) Khandogin, J.; Ziegler, T. *Spectrochim. Acta* **1999**, *55*, 607.

(79) Malkina, O. L.; Salahub, D. R.; Malkin, V. G. *J. Chem. Phys.* **1996**, *105*, 8793.

(80) Malkin, V. G.; Malkina, O. L.; Erikson, L. A.; Salahub, D. R.: In *Modern Density Functional Theory: A Tool for Chemistry*; Politzer, P., Seminario, J. M., Eds.; Elsevier: Amsterdam, 1995; pp 273-347.

(81) Breit, G. *Phy. Rev.* **1930**, *35*, 1447.

(82) Pyykkö, P.; Pajanne, E. *Phys. Lett.* **1971**, *35A*, 53.

(83) Pyykkö, P.; Pajanne, E.; Inokuti, M. *Int. J. Quant. Chem.* **1973**, *7*, 785.

(84) Pyykkö, P.; Jokisaari, J. *Chem. Phys.* **1975**, *10*, 293.

(85) Pyykkö, P. *Chem. Phys.* **1977**, *22*, 289.

(86) Pyykkö, P.; Wiesenfeld, L. *Mol. Phys.* **1981**, *43*, 557.

(87) Pyykkö, P. *J. Organomet. Chem.* **1982**, *232*, 21.

(88) Kirpekar, S.; Jensen, H. J. A.; Oddershede, J. *Theor. Chim. Acta* **1997**, *95*, 35.

(89) Boerrigter, P. M. Ph.D. thesis, Vrije University Amsterdam, 1987.

(90) Lenthe, E. v.; Baerends, E. J.; Snijders, J. G. *J. Chem. Phys.* **1993**, *99*, 4597.

(91) Bennett, B.; Rayness, W. T.; Anderson, C. T. *Spectrochim. Acta* **1989**, *45A*, 821.

(92) Dyall, K. G.; Taylor, P. R.; Faegri, K. J.; Patridge, H. *J. Chem. Phys.* **1991**, *95*, 2583.

(93) Suryanarayana, K.; Stoicheff, B. P.; Turner, R. *Can. J. Phys.* **1960**, *38*, 1516.

(94) Kashiwabara, K.; Konaka, S.; Iijima, T.; Kimura, M. *Bull. Chem. Soc. Japn.* **1973**, *46*, 407.

(95) Sequeira, A.; Chidambaram, R. *Acta Cryst.* **1965**, *20*, 910.

(96) Ziegler, B.; Babel, D. *Z. Naturforsch.* **1991**, *42b*, 47.

(97) Thiele, G.; Großmann, J.; Pürzer, A. W. *Z. Naturforsch.* **1986**, *41b*, 1346.

(98) Barandiarán, Z.; Seijo, L. *J. Chem. Phys.* **1994**, *101*, 4049.

(99) Rochon, F. D.; Melanson, R. *Acta Cryst. Sect. C* **1991**, *47*, 2300.

(100) Marriott, J. C.; Salthouse, J. A.; Ware, M. J.; Freeman, J. M. *Chem. Comm.* **1970**, *1*, 595.

(101) Hitchcock, P. B.; Jacobson, B.; Pidcock, A. *J. Organomet. Chem.* **1977**, *136*, 397.

(102) Allen, F. H.; Kennard, O.; Taylor, R. *Acc. Chem. Res.* **1983**, *16*.

(103) Millburn, G. H.; Truter, M. R. *J. Chem. Soc.* **1966**, 1609.

(104) Basch, H.; Krauss, M.; Stevens, W. J.; Cohen, D. *Inorg. Chem.* **1985**, *24*, 3313.

(105) Packett, D. L.; Jensen, C. M.; Cowan, R. L.; Strouse, C. E.; Trogler, W. C. *Inorg. Chem.* **1985**, *24*, 3578-3583.

(106) Perdew, J. P. *Phys. Rev. B* **1992**, *46*, 6671.

(107) Pyykkö, P. *Chem. Rev.* **1988**, *88*, 563.

(108) Appleton, T. G.; Clark, H. C.; Manzer, L. E. *Coordination Chemistry Reviews* **1973**, *10*, 335-422.

(109) Shustorovich, E. M.; Portai-Koshits, M. A.; Buslaev, Y. A. *Coord. Chem. Rev.* **1975**, *17*, 1-98.

(110) Pregosin, P. S.; Kunz, R. W.: In *NMR Basic Principles and Progress*; Diehl, P., Fluck, E., Kosfeld, R., Eds.; Springer-Verlag:, 1979; Vol. 16.

(111) Pregosin, P. S.: In *Annual Reports on NMR Spectroscopy*; Webb, G. A., Ed.; Academic Press: London, 1986; Vol. 17.

(112) Pidcok, A.; Richards, R. E.; Venanzi, L. M. *J. Chem. Soc. A.* **1966**, 1707.

(113) Allen, F. H.; Pidcock, A.; Waterhouse, C. R. *J. Chem. Soc. A* **1970**, 2087.

(114) Dreeskamp, H. *Z. Naturforsch.* **1964**, *19*, 139.

(115) Wilkins, A. L.; Watkinson, P. J.; MacKay, K. M. *J. Chem. Soc. Dalton Trans.* **1987**, 2365.

(116) Schumann, C.; Dreeskamp, H. *J. Magn. Reson.* **1970**, *3*, 204.

(117) Wrackmeyer, B.; Horchler, K.: In *Annual Repors in NMR Spectroscopy*; Webb, Ed.; Academic Press: London, 1989; Vol. 22.

(118) Wu, G.; Kroeker, S.; Wasylishen, R. E. *Inorg. Chem.* **1995**, *34*, 1595.

(119) Nee, M.; Roberts, J. D. *Biochem.* **1982**, *21*, 4920.

(120) Appleton, T. G.; Bailey, A. J.; Barnham, K. J.; Hall, J. R. *Inorg. Chem.* **1992**, *31*, 3077-3082.

(121) Khandogin, J. "ZORA Spin-Spin Coupling notes", August **1998**.

(122) Becke, A. *Phys. Rev. A* **1988**, *38*, 3098.

(123) Perdew, J. P. *Phys. Rev. B* **1986**, *33*, 8822.

(124) Lee, C.; Yang, W.; Parr, R. G. *Phys. Rev. B* **1988**, *37*, 785.

(125) Burdett, J. K.; Albright, T. A. *Inorg. Chem.* **1979**, *18*, 2112.

(126) Fan, L.; Ziegler, T. *J. Chem. Phys.* **1991**, *94*, 6057.